BLUFF-BODY AERODYNAMICS

Each body provided with a relative motion with respect to a fluid is subject to actions caused by the motion itself. Such actions, said fluid dynamic, depend on the properties of the fluid, the shape of the body and of its orientation.

1. Representation of fluids and their motion

Let us define as velocity vector **V** in the point P the value of the velocity of a fluid particle that occupies a P(x,y,z) at time t. The lines for which, in t, velocity vectors are tangent to them are called stream lines. The trajectories of the fluid particles are the loci of the positions occupied by the particles on varying the time.

1.1 State equations

The physical property that characterizes fluids is their lack of a defined shape and their ability to finite deformation even under the action of infinitesimal forces, if appropriately applied. More precisely, a fluid in motion is a substance that deforms continuously under the action of shear forces. On the contrary, in a fluid in quiet, or in a static equilibrium state, a fluid particle is subjected only to actions normal to its surface (pressure) and not shear (in contrast with what occurs in a solid).

The fluids can be divided into gas and liquid. The most important difference between the mechanical properties of liquids and gases is their different compressibility. The liquids may be considered, with good approximation, incompressible, so their state equation can be expressed in the form:

$$\rho = \text{constant} \tag{1.1}$$

Conversely, the state equation of gas links the change in density to those of the pressure p and the absolute temperature T. The air, in particular, can be considered a perfect gas and its state equation is:

$$p = \rho RT \tag{1.2}$$

where R is the characteristic constant of as (for dry air, R ~ 287 $m^2/ s^2/ °K$).

The variations of the specific volume of a gas in motion with velocity $V = \|\mathbf{V}\|$ become significant only if V is comparable or greater than the "speed of sound" a, namely the speed of propagation of small perturbations in the gas. It results:

$$a = \sqrt{\gamma RT} \tag{1.3}$$

where $\gamma = C_p / C_v, C_p$ is the specific heat at constant pressure, C_v is the specific heat at constant volume (for air with p = 1 atm and T = 15°C, a ~ 340.5 m/s).

Let us define as the Mach number the non-dimensional quantity:

$$M = \frac{V}{a} \qquad (1.4)$$

When M is sufficiently less than unity (e.g. M < 0.3 as it is usual in wind engineering), the gas (air) behaves as incompressible, and this entails substantial simplifications in the equations of motion.

1.2 Fluid viscosity

The shear actions acting on the fluid elements in motion are related to the tendency of the element to resist its deformation. The physical mechanism responsible for this phenomenon must be sought at the molecular level and is linked to the exchanges of momentum between layers of fluid at different speeds, caused by the motion of molecular agitation characteristic of each substance. Considering the surface AA in the fluid in Figure 1, the molecules that pass through this surface downwards have more momentum, in the direction x, of the average one of the fluid particles that meet; therefore they tend to entrain the layer of fluid below. The reverse phenomenon takes place because the molecules that cross the surface AA upwards, and therefore tend to brake the particles placed above this surface.

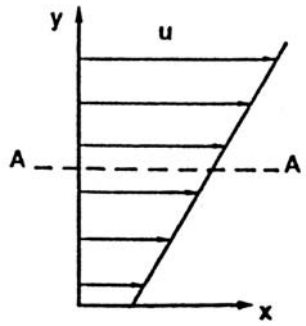

Figure 1

The entrainment and braking shear actions are then equal and opposite and the greater the greater the velocity gradient, in the two-dimensional case in Figure 1, $\partial u / \partial y$. It can be assumed that the link between that gradient and the shear stress τ is linear:

$$\tau = \mu \frac{\partial u}{\partial y} \qquad (1.5)$$

where μ is the coefficient of dynamic viscosity of the fluid that depends on the temperature because the shear action is greater the higher the speed of molecular agitation of the fluid (kinetic theory).

The fluids that satisfy Eq. 1.5 are called Newtonian and represent a good approximation of the behavior of most of the fluids of interest, including air and water.

There are fluids, such as water and especially air, with "low viscosity", that is, with small values of μ. Thus, it arises spontaneously the idea of neglecting the viscosity, introducing the concept of "non-viscous ideal fluid", that is without the inside shear action. The mathematical consequences of this hypothesis will be assessed below. By

now, however, it is possible to examine a fundamental distinction: the behavior of a non-viscous fluid and a viscous fluid at a solid boundary.

Treating the fluid as ideal, that is, non-viscous, the normal component to the solid wall of the relative velocity between the fluid and the wall is zero, that is:

$$\left(\mathbf{V} - \mathbf{V}_p\right)\bullet\mathbf{n} = 0 \qquad (1.6)$$

where $\mathbf{V}$ is the velocity of the fluid particle in contact with the wall, $\mathbf{V}_p$ is the velocity of the wall, $\mathbf{n}$ is the normal to the wall. In other words it is possible that the fluid particle has non-zero tangential velocity relative to the wall.

Experience shows that the particles of a viscous fluid in contact with a wall remain adherent to this, for which the boundary condition becomes:

$$\mathbf{V} - \mathbf{V}_p = \mathbf{0} \qquad (1.7)$$

In this case not only the normal component but also the tangential one of the relative velocity between the fluid and the wall are null. Thus, although in appearance it may seem that a fluid that almost touches a wall is provided with non-null tangential velocity, this is not true. The illusion is due to the fact that the velocity increases rapidly in a very thin layer of fluid, the "boundary layer", that separates the wall from the rest of the fluid (Figure 2).

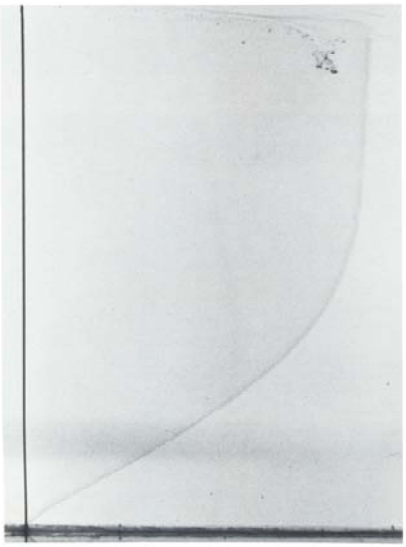

Figure 2

1.3 Description of the motion

Two possible description are possible:

a) Lagrangian description: follows the motion of the particle, whose coordinates and speed are defined as a function of time.

b) Eulerian description: analyzes the time variation of the velocity, density, pressure, etc. of the several particles that occupy fixed points in space.

Let us define as “total” or “substantial” derivative the operator:

$$\frac{D}{Dt} = \frac{\partial}{\partial t} + \mathbf{V}\bullet\mathbf{grad} \qquad (1.8)$$

The quantity $\partial / \partial t$ is the "unsteady term" and represents the variation related to the possible non-stationary field. The quantity **V•grad** is called "convective term" and is the variation over the time of a quantity associated with a particle of the fluid with velocity **V** through a spatial gradient of the same quantity.

2. Equations of motion of fluids

The writing of the equations of fluid dynamics is based on making mathematically explicit three fundamental principles of the mechanics of continuous media:

a) the law of mass conservation;

b) the theorem of momentum (or Newton's law);

c) the law of energy conservation (or the first principle of thermodynamics).

These laws should be specialized to the fluid medium in question by means of appropriate constitutive equations (state equations, equations that define the tensor of the surface stress as a function of the strain tensor, equations relating the flow of heat with the temperature field).

2.1 Equation of continuity

The equation of continuity expresses the mass conservation for a material volume of fluid, namely a volume of fluid in motion that always consist of the same particles:

$$\frac{D\rho}{Dt} + \operatorname{div}(\rho\mathbf{V}) = 0 \qquad (2.1)$$

2.2 Equation of the balance of momentum

This equation states that the time variation of the momentum of a material volume of fluid is equal to the resultant force **F** acting on it. In vector form it results:

$$\rho\frac{D\mathbf{V}}{Dt} = -\operatorname{grad} p + \rho\mathbf{f} + \operatorname{div}\boldsymbol{\tau} \qquad (2.2)$$

where p is the pressure and $\boldsymbol{\tau}$ is the vector of the shear stresses or viscous stresses.

2.3 Equation of the balance of energy

This equation expresses the principle that, in the unit time, the variation of the sum of the internal and kinetic energy for a material volume of fluid is the sum of the amount of heat input from the outside and the work done by the forces acting on the system :

$$\rho\left[\frac{\partial\left(e+V^2/2\right)}{\partial t}+\mathbf{V}\bullet\mathbf{grad}\left(e+V^2/2\right)\right]= \tag{2.3}$$
$$=\rho\mathbf{f}\cdot\mathbf{V}-\operatorname{div}\left(p\mathbf{V}\right)+\sum\nolimits_i\operatorname{div}\left(u_i\boldsymbol{\tau}_i\right)-\operatorname{div}\mathbf{q}$$

where $\mathbf{q}$ is the heat flux, $V=\|\mathbf{V}\|$, e is the inner energy for unit mass.

2.4 Constitutive equations

Eqs. (2.1)-(2.3) are a system of 5 scalar equations in 15 unknowns p, ρ, e, **V** (3), **q** (3), τ_{ik} (6 for the symmetry of the tensor). Thus, it is necessary to introduce other relationships that link with each other these quantities specifying the type of the fluid.

The first of these relationships are the state equations:

$$e=e\left(\rho,T\right) \tag{2.4}$$

$$p=p\left(\rho,T\right) \tag{2.5}$$

That link the internal energy and the pressure with the density ρ and the temperature T. In this way 2 new equations are introduced (then there are 7 equations) but also the new unknown (then there are 16 unknowns).

As a second step, let us introduce the relationships that define the viscous stress tensor as a function of the components of the strain tensor. Admitting that the fluid is Newtonian, it is assumed that the components of the viscous stress tensor are linear functions of the components of the linear strain and distortion:

$$\tau_{ik}=\frac{2}{3}\mu\operatorname{div}\mathbf{V}\delta_{ik}+\mu\left(\frac{\partial u_i}{\partial x_k}+\frac{\partial u_k}{\partial x_i}\right) \tag{2.6}$$

where δ_{ik} is Kronecker symbol. In this way the equations become 13 (7+6).

Finally, the heat flux is linked with the temperature field, assuming that it is a linear function of the temperature gradient:

$$\mathbf{q}=-K\operatorname{grad}T \tag{2.7}$$

where K is the “thermal conduction coefficient”; Eq. (2.7) is the Fourier law. At this point a system of 16 equations in 16 unknowns has been built.

However, replacing Eqs. (2.4) - (2.7) into Eqs. (2.1) - (2.3), these are reduced to a system of 5 equations in the 5 unknowns ρ, T, V. This system is often called "Navier-Stokes system", even if this name refers, more properly, to the single equation of conservation of the momentum. Now appropriate initial and boundary conditions shall be established.

The initial conditions (at time $t=t_0$) consists in the positions:

$$\rho\left(x,y,z,t_0\right)=\rho_0\left(x,y,z\right) \tag{2.8}$$

$$\mathbf{V}(x, y, z, t_0) = \mathbf{V}_0(x, y, z) \tag{2.9}$$

$$T(x, y, z, t_0) = T_0(x, y, z) \tag{2.10}$$

The boundary conditions to solve the system are 4 and relate to the temperature and speed in correspondence of the solid contour. It is assumed that in contact with the wall there is the wall temperature T. The boundary conditions for speed have already been discussed.

2.5 Equations of motion of incompressible fluids

If the fluid is incompressible (M small, ρ = constant) the continuity Eq. (2.1) becomes:

$$\text{div}\,\mathbf{V} = 0 \tag{2.11}$$

Eq. (2.11) is a linear equation in the 3 unknowns u, v, w.

The balance of the momentum (Eq. 2.12) may be written as:

$$\frac{\partial \mathbf{V}}{\partial t} + \mathbf{V} \bullet \mathbf{grad}\,\mathbf{V} = -\frac{1}{\rho}\text{grad}\,p + \mathbf{f} + \frac{\mu}{\rho}\nabla^2\mathbf{V} \tag{2.12}$$

the quantity $\nu = \mu / \rho$ being the kinematic viscosity; $\nabla^2 = \partial^2 / \partial x^2 + \partial^2 / \partial y^2 + \partial^2 / \partial z^2$ is the Laplace operator. The structure of the second term of the left hand side of the equation make it non-linear.

The physical meaning of Eq. (2.12) can be further clarified by observing that it is a Newton law (**a** = **F**/m) applied to a fluid particle. The first member is the total variation of the speed in the unit of time, decomposed in a non-stationary term and in a convective one. The second member is the force per unit of mass due to surface forces of pressure, the volume forces and the surface viscous forces ($\nu\nabla^2\mathbf{V}$). This term is in principle non-linear because μ is a function of the unknown T. However, for the incompressible fluids the variations of T are small enough to consider μ constant throughout the field.

Thus, Eqs. (2.11) and (2.12) do not contain explicitly the unknown T and so represent a system of 4 equations in the 4 unknowns 4 **V**, p. Eq. (2.3) is not needed to evaluate **V**, p. Instead, it is used to obtain T once **V**, p are known.

Let us define as vorticity vector the quantity:

$$\boldsymbol{\omega} = \text{rot}\,\mathbf{V} \tag{2.13}$$

A motion for which $\boldsymbol{\omega}$ = **0** (absence of rigid rotations) is said “irrotational”.

Let us assume that the field of the mass forces **f** is conservative (as for instance the case of the gravitational forces). Thus, let us define:

$$\mathbf{f} = -\text{grad}\,\Omega \tag{2.14}$$

Replacing Eqs. (2.13) and (2.14) into Eq. (2.12), Eq. (2.12) assumes the form:

$$\frac{\partial \mathbf{V}}{\partial t} + \boldsymbol{\omega} \wedge \mathbf{V} = -\text{grad}\left(\frac{p}{\rho} + \frac{V^2}{2} + \Omega\right) - \nu \text{ rot } \boldsymbol{\omega} \tag{2.15}$$

It points out a series of relevant conceptual properties:

a) Steady motion. Since $\partial / \partial t = 0$, Eq. (2.15) becomes:

$$\boldsymbol{\omega} \wedge \mathbf{V} = -\text{ grad}\left(\frac{p}{\rho} + \frac{V^2}{2} + \Omega\right) - \nu \text{ rot } \boldsymbol{\omega} \tag{2.16}$$

b) Ideal non-viscous fluid. Assuming $\mu = 0$ in Eq. (2.15) it follows:

$$\frac{\partial \mathbf{V}}{\partial t} + \boldsymbol{\omega} \wedge \mathbf{V} = -\text{grad}\left(\frac{p}{\rho} + \frac{V^2}{2} + \Omega\right) \tag{2.17}$$

which constitutes the Euler equation. The only hypothesis of non-viscous fluid, that is, without additional conditions on the motion, is not enough to linearize the problem (that remains non-linear due to the terms $\omega \wedge \mathbf{V}$ and V^2).

c) Irrotational motion. Since $\boldsymbol{\omega} = \mathbf{0}$, Eq. (2.15) becomes:

$$\frac{\partial \mathbf{V}}{\partial t} = -\text{grad}\left(\frac{p}{\rho} + \frac{V^2}{2} + \Omega\right) \tag{2.18}$$

which shows the disappearance of the term ν rot $\boldsymbol{\omega}$, namely of the forces caused by shear stresses of viscous nature. Thus, the equations of motion of an incompressible fluid in irrotational motion are the same for viscous and non-viscous fluids.

d) Irrotational steady motion. Eq. (2.15) becomes:

$$\frac{p}{\rho} + \frac{V^2}{2} + \Omega = \text{cos tante} \tag{2.19}$$

where the left hand side is referred to as the “Bernoulli trinomial”. Eq. (2.19) is the Bernoulli equation.

Velocity potential

The irrotationality condition $\boldsymbol{\omega} = \text{rot } \mathbf{V} = \mathbf{0}$ implies the existence of a velocity potential, i.e. of a scalar function of space φ such as:

$$\mathbf{V} = \text{grad } \varphi \tag{2.20}$$

Replacing Eq. (2.20) into the continuity Eq. (2.21) and remembering that div grad = ∇^2:

$$\nabla^2 \varphi = 0 \tag{2.21}$$

Thus, the velocity potential satisfies the Laplace equation. In other words, with the assumptions made, the system of 4 equations in the 4 unknowns V, p has been brought

back to Eq. (2.21) in the sole unknown φ. $\mathbf{V}\left(u = \partial\varphi/\partial x, v = \partial\varphi/\partial y, w = \partial\varphi/\partial z\right)$ is then derived from the solution of Eq. (2.20). Finally, p is provided by Eq. (2.19).

The simplification obtained is extraordinary: 1) Eq. (2.21) is linear; 2) it is one of the most known and studied equations of mathematical physics; 3) in the case of steady motion and irrotational and incompressible fluid, it applies to both viscous and non-viscous fluids. However, it is worth noting the question whether an irrotational motion of a viscous fluid is physically possible even in the presence of solid contours.

Consider a reference system such that the solid contours are at rest. Assuming that the fluid is viscous (Eq. 1.5), the particles in contact with the wall have null velocity ($\mathbf{V} = \mathbf{0}$); therefore, for the hypothesis of irrotationality, grad φ = 0 (Eq. 2.20). With this boundary condition, the Laplace Eq. (2.21) admits the unique solution φ = constant all over the field, and therefore $\mathbf{V} = \mathbf{0}$ everywhere. In other words, in the presence of solid contours a viscous fluid cannot possess an irrotational motion.

Conversely, if the fluid is non-viscous (Eq. 1.6), the particles in contact with the wall may have tangential components of the velocity ($\mathbf{V} \bullet \mathbf{n} = 0$); so, by virtue of Eq. (2.20), $\text{grad}\,\varphi \bullet \mathbf{n} = 0$ or $\partial\varphi/\partial n = 0$. Thus, the Laplace equation has only one solution that corresponds to a non-null velocity field. In other words, in the presence of solid contours the hypotheses of non-viscous fluid and irrotational motion are perfectly compatible.

2.6 Equations of motion of non-viscous fluids

The hypothesis of non-viscous fluid (Eq. 2.17) has been the basis of nearly all the theoretical work done in the nineteenth century. This was due not only to the obvious simplification of the mathematical treatment, but also to some physical considerations apparently faulted.

Taking into consideration the equation of motion (2.12), the order of magnitude of the inertial force is that of the term $\rho\mathbf{V} \bullet \text{grad}\,\mathbf{V}$, i.e. $\rho V^2 / L$. The order of magnitude of the viscous force is instead $\mu\nabla^2\mathbf{V}$, i.e. $\mu V / L^2$. The ratio of the order of magnitude of the inertial force and the viscous force is identified with the Reynolds number:

$$\text{Re} = \frac{\rho V L}{\mu} = \frac{V L}{\nu} \tag{2.22}$$

where V and L are a velocity and a length characteristic of the problem. In most problems of practical interest, and in particular in the evaluation of the aerodynamic wind actions on buildings, the Reynolds number is in the order of 10^6 - 10^8. Thus, neglecting the viscous forces with respect to the inertial ones is an approximation seemingly reasonable.

Consider a body immersed in a non-viscous fluid in a relative motion with respect to the body and solve the Laplace Eq. (2.21) with the boundary condition $\partial\varphi/\partial n = 0$ (on the surface of the body). From φ determine the velocity field and from this, with

the Bernoulli Eq. (2.19), the state of pressure on the surface of the body. It is shown that the integral of the pressures on the surface of the body has a null resultant, which constitutes the D'Alembert paradox.

This result is in marked contrast to the experience showing that a body moving in a fluid is subject to a force, which is opposed to its progress.

Synthesizing the above concepts, the motion of viscous fluids cannot be completely irrotational in the presence of solid contours; this derives from the need of satisfying the boundary condition of no slip at the wall. However, this does not prevent the existence of irrotational motions in field areas sufficiently far from solid boundaries. One might even imagine the existence of flow fields in which the vorticity is limited to areas close to solid contours while in the outside space the motion is irrotational and thus describable by the typical equations of non-viscous fluids.

3. Boundary layer

The concept of a thin layer of fluid near the solid boundary in which vorticity is contained and outside of which the flow can be considered as irrotational was introduced by Prandtl in 1904. He called this layer "boundary layer".

Figure 3 provides in schematic form the illustration in Figure 2: u represents the velocity relative to a plan solid contour, δ is the thickness of the boundary layer, u_e is the velocity of the fluid at the top of the boundary layer.

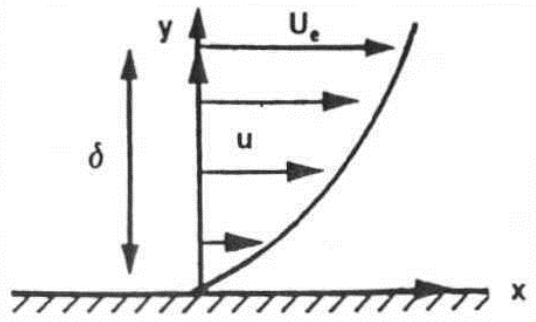

Figure 3

Figure 4 shows the boundary layer around a body (said aerodynamic). The dotted line indicates the outer edge of the boundary layer where the speed has the value u_e that can be derived from the solution of the Laplace equation, valid in the irrotational field.

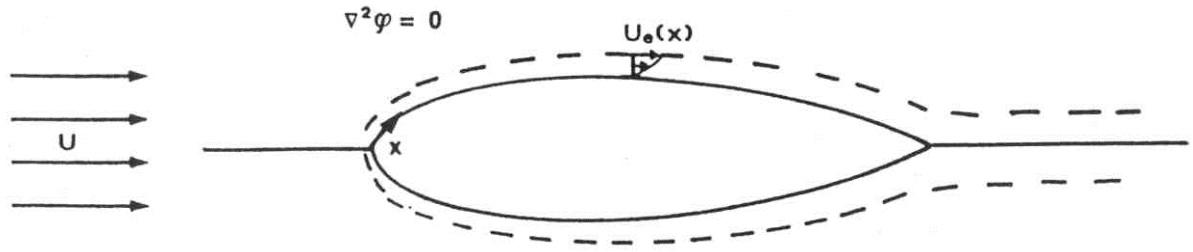

Figura 4

The thickness of the boundary layer is given by:

$$\frac{\delta}{L} \cong \left(\frac{1}{Re}\right)^{1/2} \tag{3.1}$$

where L is a characteristic length of the body. Since Re is usually large, the boundary layer is very thin (Figure 4 is clearly off-scale).

The variation of the pressure p in the boundary layer is negligible ($\partial p / \partial y \cong 0$), so the pressure at a point of the surface of a body is approximately the same in the fluid at the outer edge of the boundary layer, above the point considered. As such it may be obtained by means of the Bernoulli equation.

3.1 Laminar and turbulent boundary layer

Until now it was assumed that the individual fluid particles move parallel to the surface of the body. This model refers in reality to the situation of “laminar” flow (Figure 2). Experience shows that with the increase of the Reynolds number (suitably calculated) the boundary layer tends to become “turbulent” (Figure 5).

Figure 5

Referring to Figure 4, x is a curvilinear coordinate which develops along the surface of the body from the point of stagnation, i.e. from the point where the boundary layer itself begins. It defines a Reynolds $(Re)_x$ number such that:

$$(Re)_x = \frac{Ux}{\nu} \tag{3.2}$$

where U is the velocity upstream of the body. The boundary layer remains laminar up to values of x such that $(Re)_x$ is 10^5-10^6. From here on it becomes turbulent.

The transition from the laminar to the turbulent flow does not occur in a precise point, but in a "transition zone". It originates as a form of instability due to several factors: a) the roughness of the wall tends to anticipate the transition; b) the pressure gradient along the wall, tends to anticipate the transition if it is positive (the external current decelerates) and delaying it if it is negative (the external current accelerates).

The turbulent flow is characterized by a deep mixing of the fluid which generates boundary layers with a thickness greater than laminar. This mixing causes random fluctuations of the speed that overlap the mean value.

3.2 Separation of the boundary layer

Consider the two-dimensional body in Figure 6. Assuming as high the Reynolds number, the trend of the pressure on its surface can be approximated by means of the potential flow theory, neglecting the boundary layer.

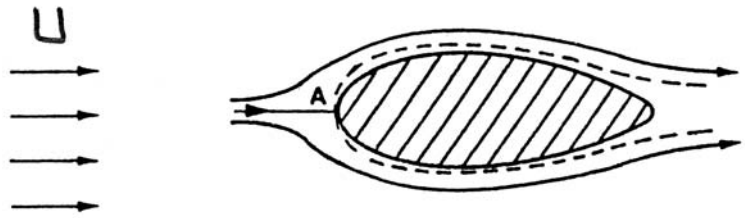

Figure 6

In the stagnation point A, for the Bernoulli equation, the pressure is maximum: $p_A = p_\infty + \rho U^2 / 2$, where U and p_∞ are the speed and the pressure of the undisturbed flow.

Along the surface, starting from A, the flow (outside the boundary layer) accelerates and the pressure decreases $(\partial p / \partial x < 0)$ up to about the zone where the body has the maximum thickness. From here on, the speed decreases and the pressure increases $(\partial p / \partial x > 0)$.

It is demonstrated that when a boundary layer is subjected to a negative pressure gradient in the direction of the wall, that is, when the external flow accelerates, its thickness decreases and its vorticity is transported toward the wall. The boundary layer is therefore "squashed" against the wall.

The opposite phenomenon occurs when a boundary layer is subjected to a positive pressure gradient along the wall, said "adverse pressure gradient". In this case the thickness of the boundary layer increases rapidly and the vorticity is transported outside up to cause the "boundary layer separation".

Figure 7 shows a typical evolution of the boundary layer along a curved wall. The internal profile of the speed changes up to the point S, said "point of boundary layer separation", where $\partial u / \partial y = 0$ on the wall. Downstream of S a retrograde flow arises at the surface and the flow field external to the boundary layer is moved away from the wall. The vorticity is thus no longer confined at the wall, but occupies a large area of the field. Figure 8 shows the laminar separation (a) and the turbulent one (b).

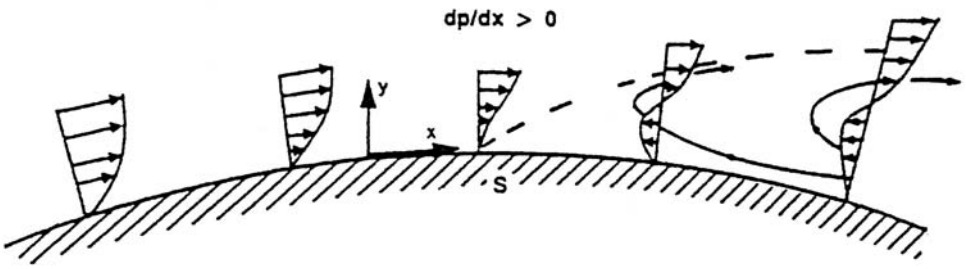

Figure 7

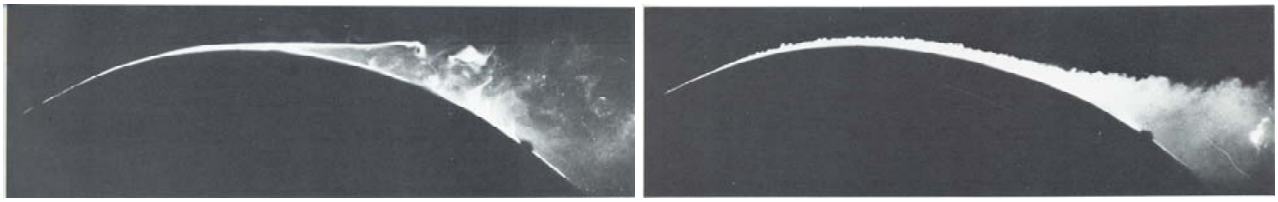

Figure 8

Downstream of S the boundary layer theory is no longer applicable and the pressure distribution provided by the theory neglecting the potential vorticity is unacceptable.

The existence of an adverse pressure gradient is a necessary condition to obtain the separation of the boundary layer.

Turbulent boundary layers are more resistant to separation than laminar ones. It is even possible the formation of "separation bubbles" (Figure 9): the laminar boundary layer becomes turbulent after separating and is thus able to reattach to the surface.

In correspondence with the corners there is always a separation of the boundary layer (Figure 10) since, if the flow was able to follow the edge, the external speed would be very high (theoretically infinite) and pressure very low. Immediately after, a very high adverse pressure gradient would occur, unsustainable without separation.

Figure 9

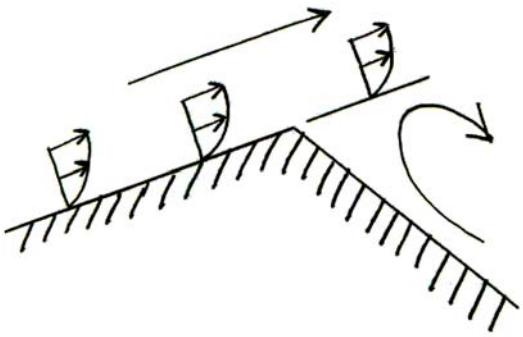

Figure 10

3.3 La scia vorticosa

Consider the classical case of the circular cylinder. For Re = UD/ν <1 (D is the diameter of the cylinder), the laminar boundary layer is attached to the cylinder along the entire perimeter (Figure 11(a)); the flow tends to wrap the body. For 1 <Re <30, the boundary layer remains laminar but is separated from the cylinder giving rise to two large stationary symmetric laminar vortices (Figure 11(b)). For 30 <Re <10000, the boundary layer is still laminar; the vortices remain laminar but are detached from the cylinder alternately realizing the Von Karman wake, i.e. two trains of vortices (Figure 11(c)) with travelling speed relative to the cylinder (Figure 12). For 10000 <Re <200000, the boundary layer remains laminar, but the vortices have a structure mainly turbulent, with layers whirling difficult to detect (Figure 11(d)). For Re> 200 000 (Figure 11(e)), the boundary layer gradually becomes turbulent (it is totally turbulent from Re ≅ 500000); simultaneously, the separation points move downward and the wake, still turbulent, tends to be ever closer.

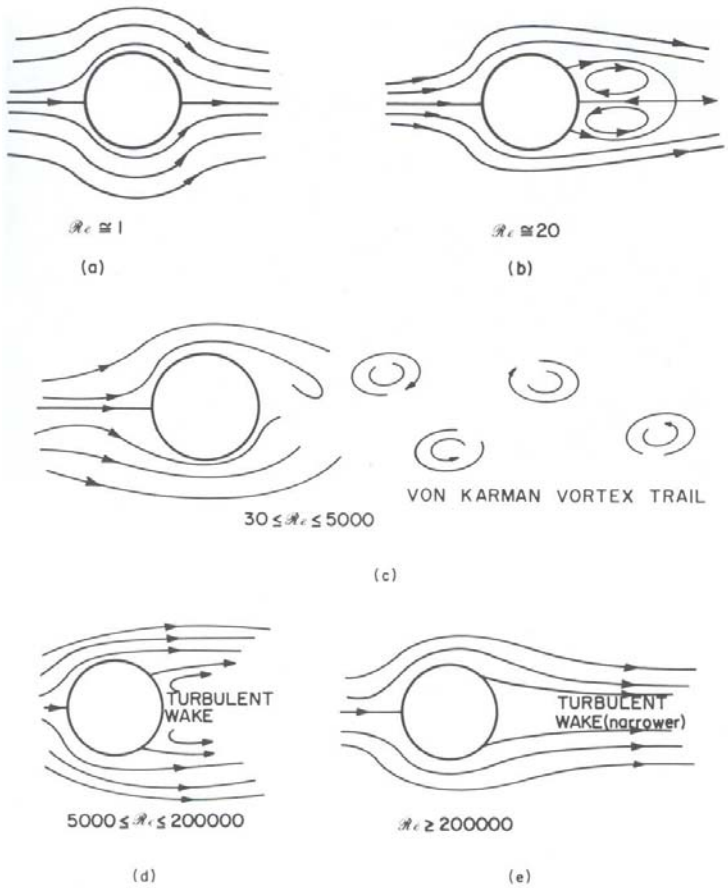

Figure 11

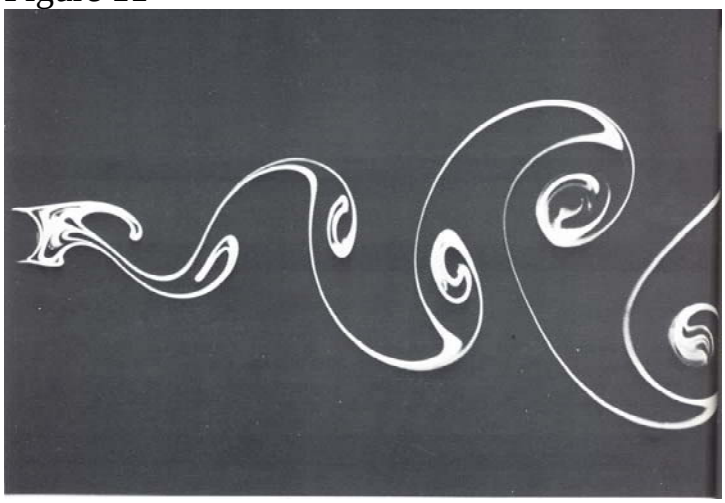

Figure 12

It can be shown that the greater the ratio between the width of the wake and the transverse size of the body, the greater is its resistance offered to the fluid.

The regularity of the vortex wake was noticed first by Strouhal in 1878. He observed that the vortex shedding can be described by a dimensionless number S, hereinafter called the Strouhal number, provided by the relationship:

$$S = \frac{nD}{U} \tag{3.3}$$

where n is the vortex shedding frequency and D is a characteristic size. S depends on the general by the shape of the cross-section of the cylinder and on the Reynolds number. Figure 13 shows some measurements of S on cylinders with circular section. Figure 14 lists the values of S relative to elongated bodies of varying shape.

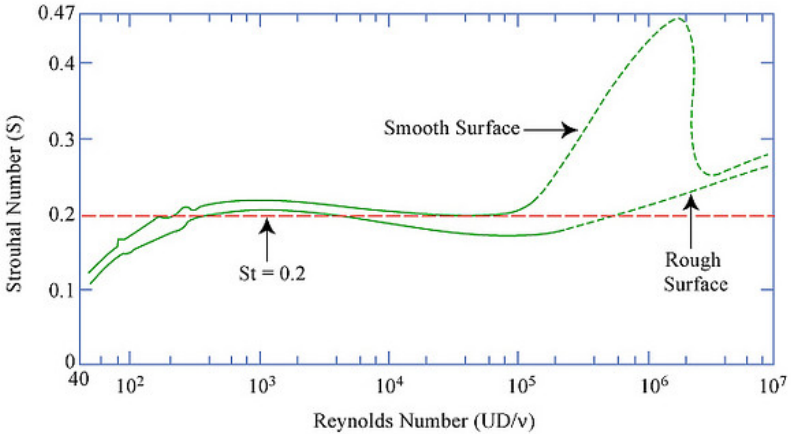

Figure 13

Wind	Profile dimensions, in mm	Value of $\mathscr{S}$	Wind	Profile dimensions, in mm	Value of $\mathscr{S}$
→	t = 2.0; 50; t; t; 50	0.120	↓	t = 1.0; 12.5; 12.5; 25; 50	0.147
↓		0.137			
→	t = 0.5; 25; 25	0.120	↓	t = 1.0; 12.5; 12.5; 12.5; 50	0.150
↓	t = 1.0; 25; 50	0.144	←	t = 1.0; 50; 50	0.145
			↑		0.142
			↙		0.147
↓	t = 1.5; 12.5; 50	0.145	←	t = 1.0; 25; 25	0.131
			↑		0.134
			↙		0.137
↓	t = 1.0; 25; 50	0.140	→	t = 1.0; 25; 25; 25; 25	0.121
↑		0.153	↓		0.143
↓	t = 1.0; 12.5; 50	0.145	→	t = 1.0; 25; 25; 25; 12.5	0.135
↑		0.168			
→	t = 1.5; 50	0.156	→	t = 1.0; 50; 100	0.160
↓		0.145			
Cylinder 11 800 < $\mathscr{R}_e$ < 19 100; 25		0.200	→	t = 1.0; 25; 50	0.114
			↑		0.145

Figure 14

The alternating shedding of vortices cause asymmetries of the velocity and pressure fields of the fluid, responsible for transversal and longitudinal forces that vary in time with frequency respectively equal and twice that of vortex shedding. The longitudinal forces are usually small. The transversal forces are often essential for the study of the behavior of buildings in respect of the wind.

The necessary condition to have a regular and alternating shedding of vortices from a two-dimensional cylinder is that the lines of separation are rectilinear, i.e. parallel to the cylinder axis. This suggests how to make the wake chaotic, and thus reducing the lateral forces, causing artificially the separation along not straight lines (Figure 15).

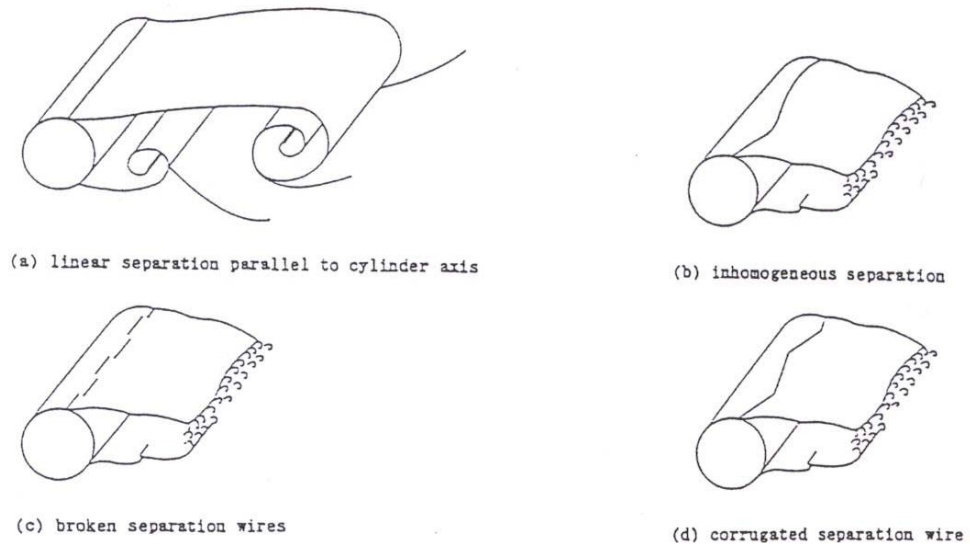

Figure 15

Another way of modifying and even inhibiting the regular and alternating shedding of vortices is to "force" the formation of a symmetric fluid field (Figure 16), by inserting downstream of the cylinder a plate parallel to the current ("splitter plate") sufficiently long to facilitate the reattachment of the fluid on its surface and the formation of a pair of stationary and symmetrical vortices. The extrapolation of this principle explains the tendency of elongated bodies to manifest vortex wakes subtle and evanescent.

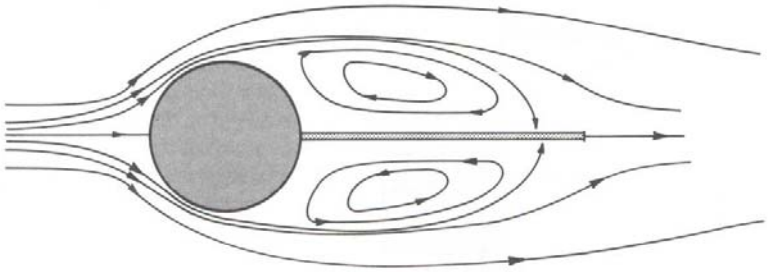

Figure 16

As an example, a square section shows the formation of a wide turbulent wake (Figure 17 (a)). Differently, for a rectangular elongated section (Fig. 17 (b)), the separation at the front edges is followed by the phenomenon of the “flow reattachment” and by a second separation at the rear edges with the formation of a very narrow wake.

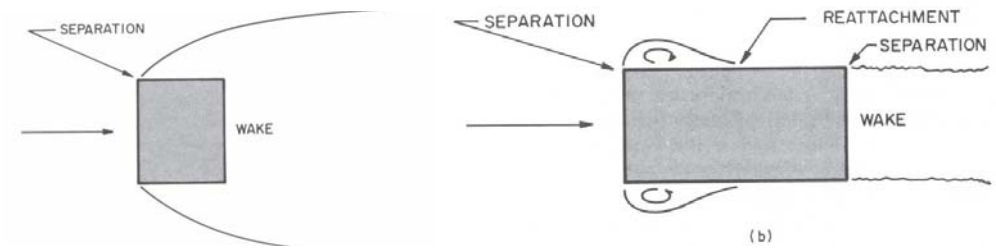

Figure 17

3.4 Aerodynamic and bluff-bodies

Let us define as aerodynamic the bodies whose boundary layer remains attached over their entire surface, except at the most small separation bubbles. They include "low incidence" airfoils (Figure 18). Their size in the flow direction is much greater than their transverse size. The wake downstream of the body is as thin as the thickness of the boundary layer. Therefore, their resistance to fluid is very reduced.

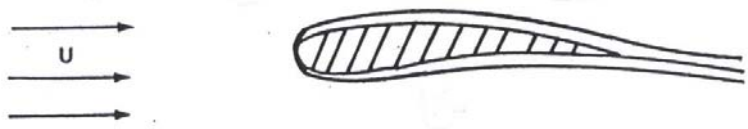

Figure 18

The bluff bodies (Figure 19) are characterized by the separation of the boundary layer from the surface and the formation of turbulent and non-steady wakes whose width has in general the same order of magnitude as the transverse size of the body. The aerodynamic drag is one or two orders of magnitude greater than that of airfoils with equal cross-sectional size (Figure 20). A "high incidence" airfoil is a bluff body.

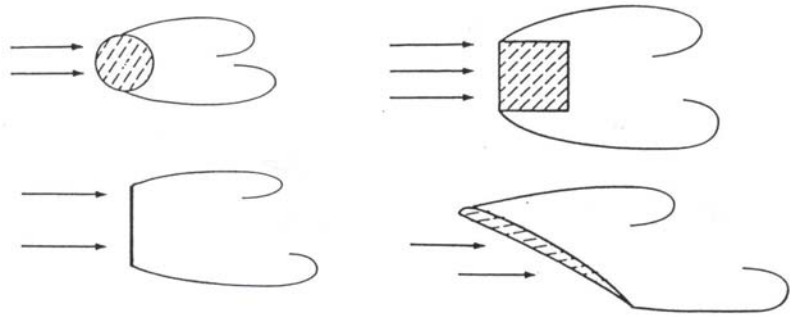

Figure 19

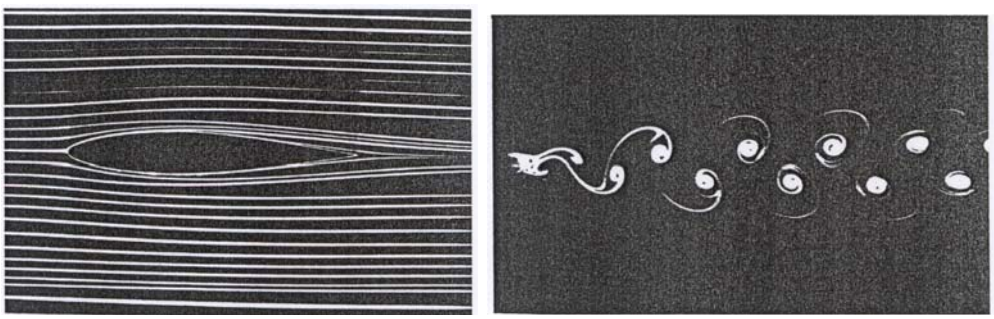

Figure 20

4. Aerodynamic actions

A body immersed in a flow field is subjected to aerodynamic actions. They depend on the speed of the flow, and the shape, size and orientation of the body. For bodies with rounded surfaces, they are also closely associated to the Reynolds number and the surface roughness.

Let U be the velocity of the undisturbed flow (upstream of the body or in body position if this were absent). Let p_o be the pressure of the undisturbed flow, defined ambient pressure or reference pressure. The wind velocity pressure of the undisturbed flow is given by:

$$q = \frac{1}{2}\rho U^2 \qquad (4.1)$$

The aerodynamic coefficients are dimensionless quantities that transform the velocity pressure q into aerodynamic actions. They are divided into 5 categories:

- *Pressure coefficients*: transform the velocity pressure q into pressures on one face of a surface;
- *Net pressure coefficients*: transform the velocity pressure q into global pressures on a surface;
- *Resultant action coefficients*: transform the velocity pressure q into resultant forces and moments on a compact body;
- *Resultant action coefficients per unit length*: transform the velocity pressure q into a force and a torsional moment per unit length;
- *Shear coefficients*: transform the velocity pressure q into shear stresses on one face of a surface parallel to the wind direction.

4.1 Pressure on one face of a surface

Let p be the pressure on a single face of the surface of a body. If $p > p_o$, it acts toward the surface (Figure 21a) and the change in pressure, $(p-p_o) > 0$, is said overpressure. If $p < p_o$, it "attracts" or "sucks" the surface toward the flow (Figure 21b) and the change in pressure, $(p-p_o) < 0$, is said depression or suction.

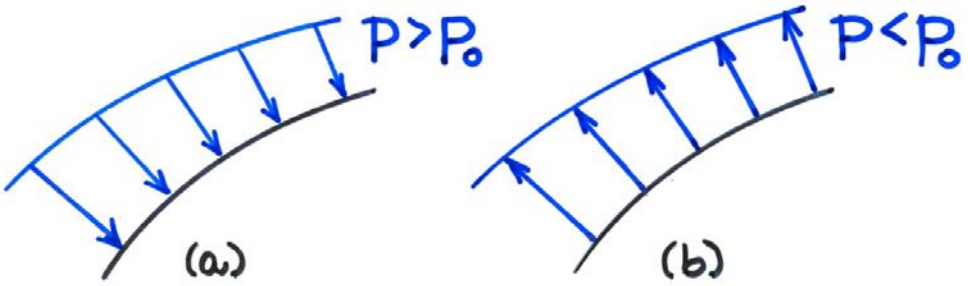

Figure 21

Let us define as external pressure p_e the pressure p exerted by the flow on one face of the outer surface of the body. Let us define as internal pressure p_i the pressure p exerted by the fluid on one face of the inner surface of the body. The direction of the pressure on the inner and outer surface has an essential role in the evaluation of the resulting action (Figure 22).

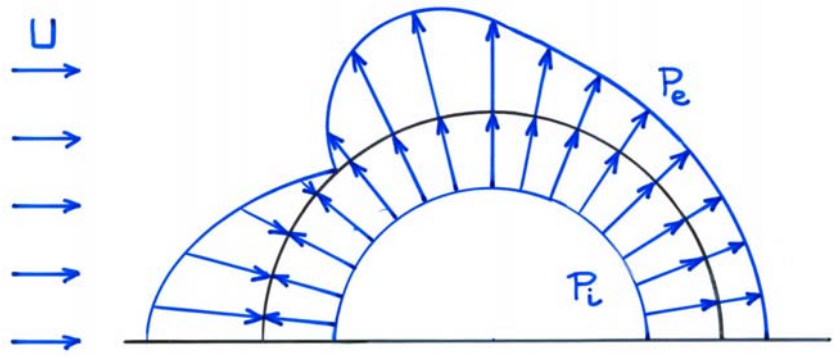

Figure 22

The distribution of the pressure p is defined through the point values of the pressure coefficient C_p. It is given by:

$$C_p = \frac{p - p_o}{\frac{1}{2}\rho U^2} \qquad (4.2)$$

The pressure coefficients on the outer face of the surface are said external pressure coefficients C_{pe}. The pressure coefficients on the inner face of the surface are said internal pressure coefficients C_{pi}. Positive values of C_p indicate actions towards the surface; negative values of C_p indicate suctions mainly associated to areas of flow separation (Figure 23).

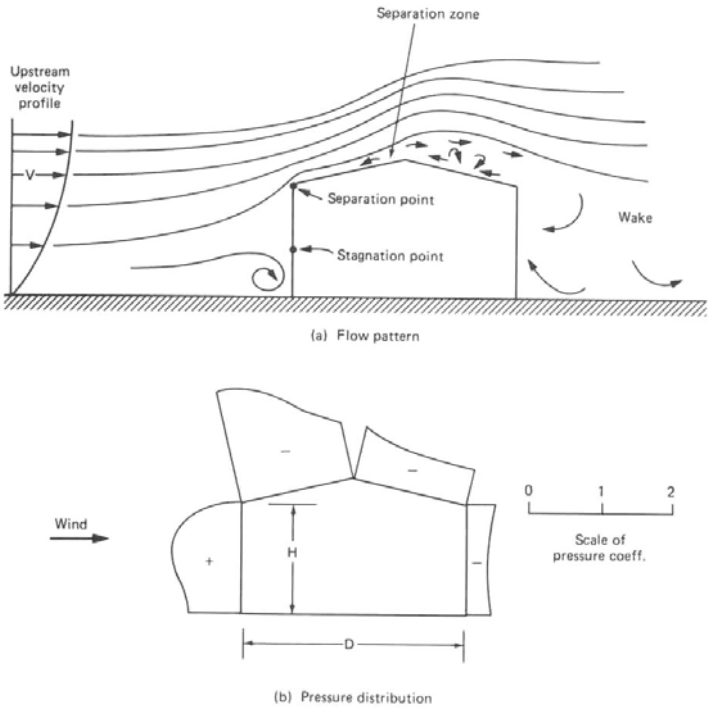

Figure 23

The pressure coefficients, measured by tests in a wind tunnel or obtained by means of CFD codes, are used to obtain p as a function of U. It follows:

$$\left(p_e - p_o\right) = \frac{1}{2}\rho U^2 C_{pe} = qC_{pe} \tag{4.3a}$$

$$\left(p_i - p_o\right) = \frac{1}{2}\rho U^2 C_{pi} = qC_{pi} \tag{4.3b}$$

The engineering practice often confuses the over-pressure (p_e-p_o) with p_e and the depression (p_i-p_o) with p_i.

4.2 Net pressure on a surface

When it is not necessary to know the aerodynamic actions on each single face of a surface, they are expressed by means of the overall pressure p_n (Figure 24). It is defined as positive or negative depending on the choice of a conventional direction.

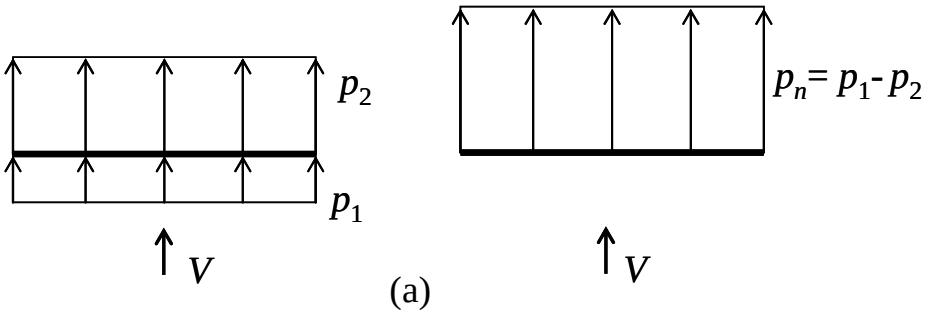

Figure 24

Assuming, for example, the positive direction of the overall pressure concordant with the overpressure (positive) on the face 1, it is expressed by the relationship:

$$p_n = \left(p_1 - p_o\right) - \left(p_2 - p_o\right) = p_1 - p_2 \tag{4.4.}$$

The distribution of p_n on the surface of the body is defined by the point values of the overall pressure coefficient C_{pn}. It is provided by the relationship:

$$C_{pn} = \frac{p_n}{\frac{1}{2}\rho U^2} \tag{4.5}$$

The net pressure coefficients, measured by tests in the wind tunnel or obtained by means of CFD codes, are used to obtain p_n as a function of U. It results:

$$p_n = \frac{1}{2}\rho U^2 C_{pn} = qC_{pn} \tag{4.6}$$

Finally, from the above relationships it follows:

$$C_{pn} = C_{p1} - C_{p2} \tag{4.7}$$

4.3 Resultant actions on a compact body

For compact bodies it is often not necessary to know the pressure distribution on their surface. In this case, the aerodynamic actions are expressed by means of the three Cartesian components of the resultant force and moment (Figure 25).

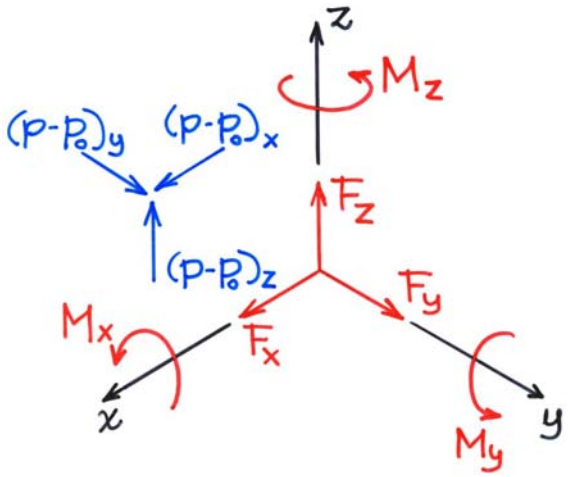

Figure 25

F_x, F_y and F_z are the three components of the resultant force along axes x, y and z; M_x, M_y and M_z are the three components of the resultant moment around axes x, y and z. They are linked to the point distribution of pressure through the relationships:

$$F_\alpha = \int_S (p - p_o)_\alpha \, dS \quad (\alpha = x, y, z) \tag{4.8}$$

$$M_x = \int_S \left[y(p - p_o)_z - z(p - p_o)_y \right] dS \tag{4.9a}$$

$$M_y = \int_S \left[z(p - p_o)_x - x(p - p_o)_z \right] dS \tag{4.9b}$$

$$M_z = \int_S \left[x(p - p_o)_y - y(p - p_o)_x \right] dS \tag{4.9c}$$

where $(p-p_o)_\alpha$ is the component of $(p-p_o)$ along α = x, y, z; x, y, z are the distances of the application point of $(p-p_o)$ from the origin of the axes; S is the body surface.

Let us define as the force coefficients, C_{fx}, C_{fy} and C_{fz}, and the moment coefficients, C_{Mx}, C_{My} and C_{Mz}, the six non-dimensional quantities:

$$C_{F\alpha} = \frac{F_\alpha}{\frac{1}{2}\rho L^2 U^2} \quad (\alpha = x, y, z) \tag{4.10}$$

$$C_{M\alpha} = \frac{M_\alpha}{\frac{1}{2}\rho L^3 U^2} \quad (\alpha = x, y, z) \tag{4.11}$$

where L is a characteristic size of the body (L is squared in (4.10) and at the cube in (4.11)). The coefficients $C_{F\alpha}$ and $C_{M\alpha}$ are linked to the external pressure coefficients $C_p = C_{pe}$ through the relationships:

$$C_{F\alpha} = \frac{1}{L}\int_S C_{p\alpha} dS \quad (\alpha = x, y, z) \tag{4.12}$$

$$C_{Mx} = \frac{1}{L^2}\int_S \left(yC_{pz} - zC_{py} \right) dS \tag{4.13a}$$

$$C_{My} = \frac{1}{L^2}\int_S \left(zC_{px} - xC_{pz} \right) dS \tag{4.13b}$$

$$C_{Mz} = \frac{1}{L^2}\int_S \left(xC_{py} - yC_{px} \right) dS \tag{4.13c}$$

where $C_{p\alpha}$ is the component of C_p along α = x,y,z.

The force and moment coefficients, measured by tests in the wind tunnel or obtained by means of CFD codes, are used to derive F and M as a function of U. It results:

$$F_\alpha = \frac{1}{2}\rho L^2 U^2 C_{F\alpha} \quad (\alpha = x, y, z) \tag{4.14}$$

$$M_\alpha = \frac{1}{2}\rho L^3 U^2 C_{M\alpha} \quad (\alpha = x, y, z) \tag{4.15}$$

4.4 Resultant action per unit length on an elongated body

For elongated bodies it is often not necessary to know the pressure distribution on their contour. In this situation the aerodynamic actions are expressed as forces and moments per unit length (Figure 26).

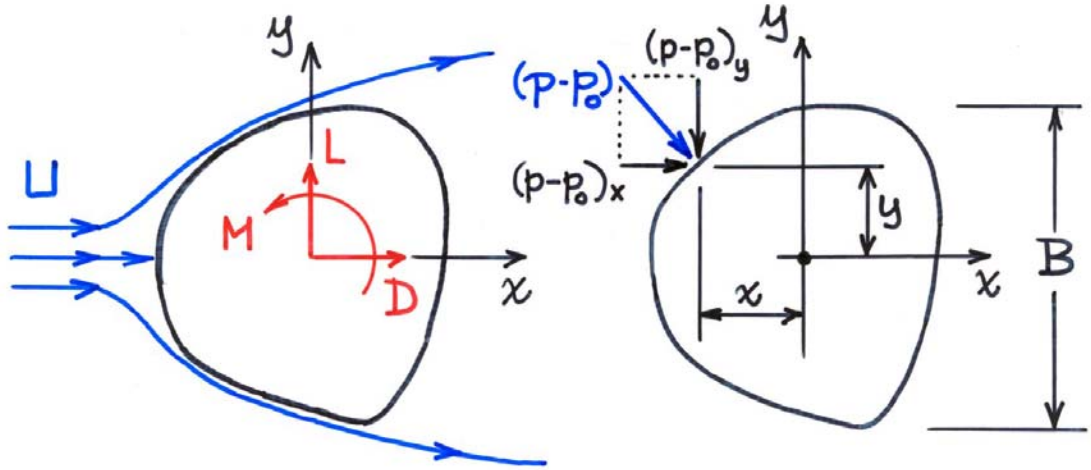

Figure 26

Examining Figure 26(a), D is the force per unit length in the flow direction, or "drag"; L is the force per unit length perpendicular to the flow direction, or "lift"; M is the torsional moment per unit length around the axis normal to the cross-section (in the plane containing D and L). These actions are associated with the pressure distribution by the relationships:

$$D = \int_s (p - p_o)_x ds \tag{4.16a}$$

$$L = \int_s (p - p_o)_y ds \tag{4.16b}$$

$$M = \int_s \left[x(p - p_o)_y - y(p - p_o)_x \right] ds \tag{4.16c}$$

where $(p\text{-}p_o)_x$ and $(p\text{-}p_o)_y$ are the components of $(p\text{-}p_o)$ along D (x) and L (y); x and y are the distances of the point of application of $(p\text{-}p_o)$ from the origin of axes; s is the contour of the section (Figure 26b).

Let us define the drag coefficient C_D, the lift coefficient C_L and the torsional moment coefficient C_M as the three dimensionless quantities:

$$C_D = \frac{D}{\frac{1}{2}\rho B U^2} \tag{4.17a}$$

$$C_L = \frac{L}{\frac{1}{2}\rho B U^2} \tag{4.17b}$$

$$C_M = \frac{M}{\frac{1}{2}\rho B^2 U^2} \tag{4.17c}$$

where B is a characteristic length of the cross-section (Figure 26) (B at the square in Eq. 4.15c). The coefficients C_D, C_L and C_M are linked to the external pressure coefficients through the relationships:

$$C_D = \frac{1}{B}\int_s C_{px}\, ds \tag{4.18a}$$

$$C_L = \frac{1}{B}\int_s C_{py}\, ds \tag{4.18b}$$

$$C_M = \frac{1}{B^2}\int_s \left(xC_{py} - yC_{px} \right) ds \tag{4.18c}$$

where C_{px} and C_{py} are the components of C_p along D (x) and L (y).

The force and moment coefficients per unit length, measured by means of tests in the wind tunnel or obtained by means of CFD codes, are used to obtain D, L and M as a function of U. it follows that:

$$D = \frac{1}{2}\rho B U^2 C_D \tag{4.19a}$$

$$L = \frac{1}{2}\rho B U^2 C_L \tag{4.19b}$$

$$M = \frac{1}{2}\rho B^2 U^2 C_M \tag{4.19c}$$

4.5 Shear actions

For bodies with large surfaces it is necessary to take into account the shear actions exerted by the wind on the surfaces parallel to the flow direction (Figure 27).

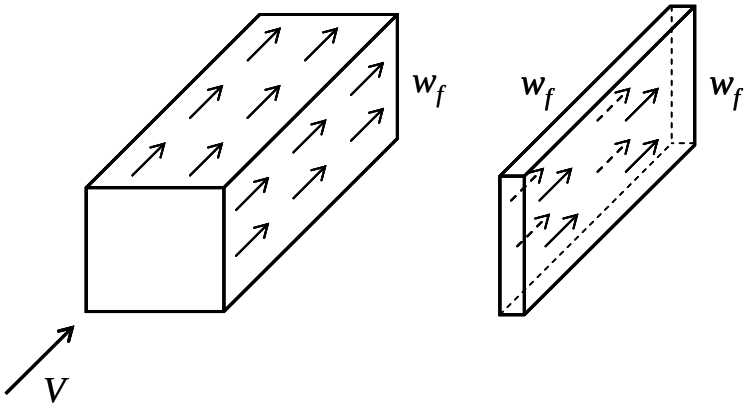

Figure 27

The distribution of the shear stresses w_f on a face of the surface is defined by means of the point values of the shear coefficient C_f It is provided by the relationship:

$$C_f = \frac{w_f}{\frac{1}{2}\rho U^2} \tag{4.20}$$

The knowledge of the shear coefficients allows to derive, knowing U, the distribution of the shear stress w_f on a face of the surface. In particular:

$$w_f = \frac{1}{2}\rho U^2 C_f = qC_f \tag{4.21}$$

4.6 Variability of the undisturbed flow speed and aerodynamic actions

The speed U of the undisturbed flow that appears in all the previous equations is actually often variable over time and space. When U varies in time, for example because of atmospheric turbulence, it is normally interpreted as the mean value of the speed (except in cases where it is identified with the peak value $\hat{u}$). When U varies in space (for example according to the profile of the mean wind speed), there are two possible conventions: the first uses the value of U at the height z of the aerodynamic action (Figure 28), the second uses the value of U at a fixed reference height z_{ref} (Figure 29).

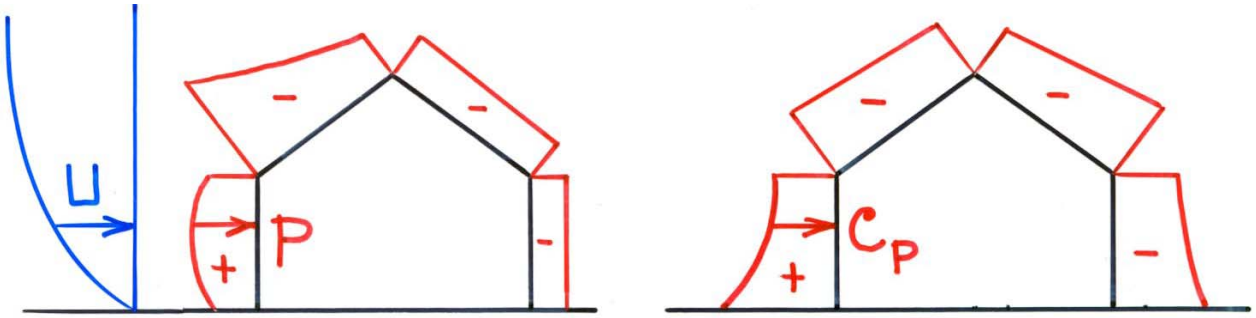

Figure 28

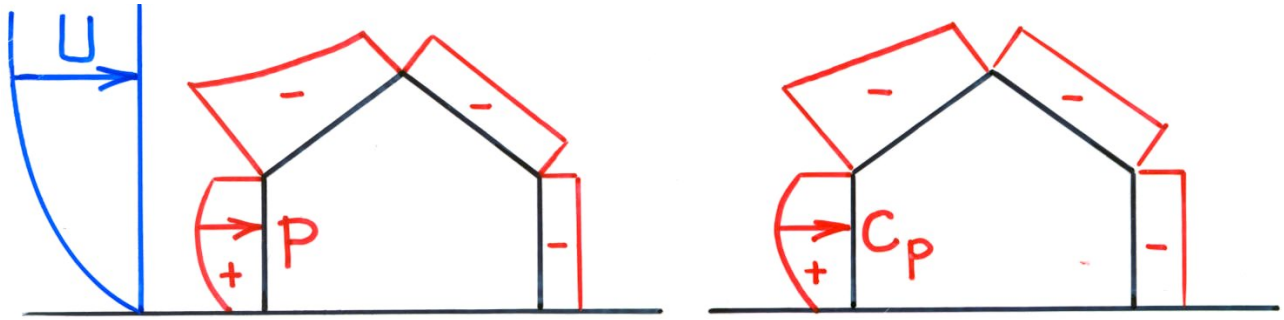

Figure 29

The aerodynamic action generally varies in time and is then decomposed, as the wind speed, in a constant mean part and a nil mean fluctuation (Figure 30). The fluctuating component can be represented by quantities such as the standard deviation, the peak value, the power spectrum, the skewness and the kurtosis.

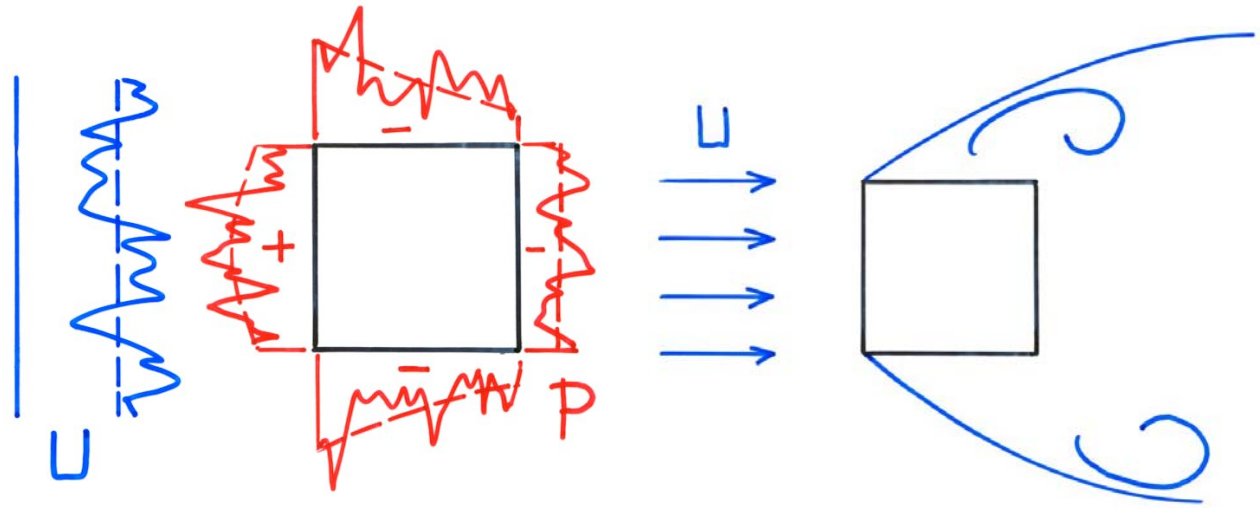

Figure 30

The presence of fluctuating actions is caused by the turbulence of the oncoming flow (Figure 30a) or by the vortex wake produced by the body itself (Figure 30b).

One can therefore say that the case of the aerodynamic actions independent of time is realized only for small incidence airfoils in smooth flows. In all other situations the actions vary in time. The definition of the aerodynamic coefficients therefore requires some clarification.

Let us define as mean aerodynamic coefficients $\bar{C}$ the dimensionless quantities introduced above associated with the mean values of the aerodynamic actions; where there is no ambiguity they are called more simply aerodynamic coefficients. Let us define as rms ("root mean square") $\tilde{C}$ aerodynamic coefficients those associated with the standard deviations of the fluctuating aerodynamic actions. Let us define as maximum $\hat{C}$ and minimum $\breve{C}$ peak aerodynamic coefficients those calculated at the maximum and minimum values of the aerodynamic actions.

5. One-dimensional bodies

Let us define as one-dimensional a body with ideally infinite length and compact cross-section, immersed in a uniform flow orthogonal to its axis line. In this case the flow field has two-dimensional characteristics in the plane orthogonal to the axis line. This representation is often used to schematize the structures or structural elements sufficiently elongated or comprised between two parallel walls perpendicular to their axis ("end plates").

The aerodynamic coefficients of these bodies depend on various parameters such as the shape of the cross-section and its orientation, the Reynolds number, the surface roughness and the turbulence intensity (strictly speaking, the turbulence makes the problem three-dimensional). To frame comprehensively this topic is impossible. Below it is then given a set of patterns that constitute preliminary references.

Figure 31 shows the drag coefficient of a smooth circular cylinder in a laminar flow, as a function of the Reynolds number. For Re < 200000 (Figure 11a-d), in the so-called sub-critical domain, the boundary layer remains laminar, the drag is maximum, C_D is about 1.2. For 200000 < Re < 500000, in the critical domain, the boundary layer becomes turbulent, the separation point moves downstream (Figure 32), the wake becomes narrower and chaotic (Figure 14c), the drag "collapses" (C_D is equal to about 1/3 of that in the sub-critical domain). For Re > 500000, in the super-critical domain, the vortex shedding recovers regularity and the drag increases again though remaining much smaller than in the sub-critical domain. Figure 33 illustrates the transition from the sub-critical to the super-critical domain through the distribution of the pressure coefficient along the circumference of the cylinder.

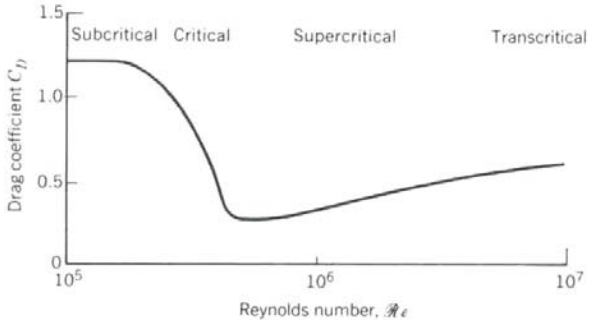

Figure 31

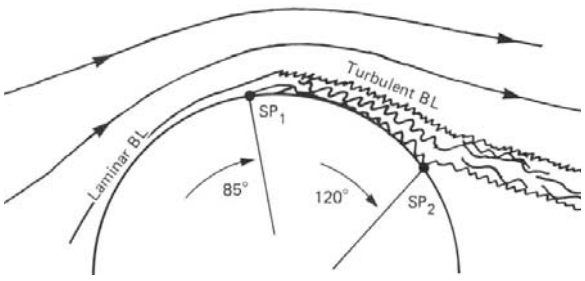

Figure 32

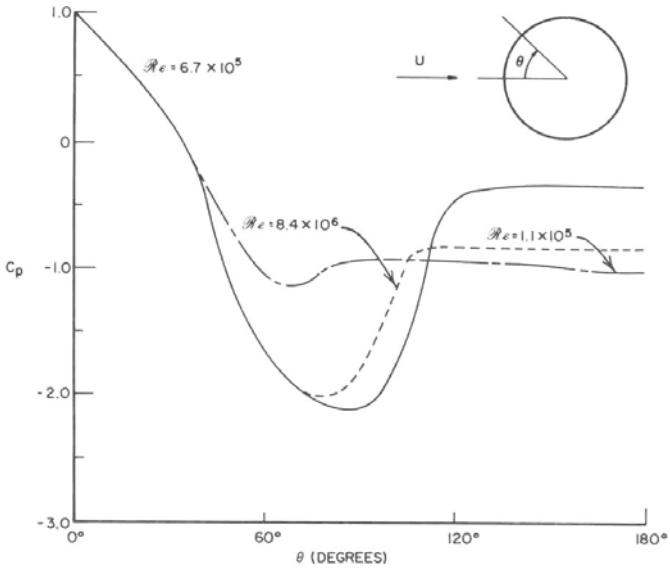

Figure 33

Figure 34 shows typical flow regimes in the neighborhood of cylinders with square and rectangular cross-section. The wake separation occurs at the sharp edges of the section. It follows that the physical phenomenon becomes almost independent of the Reynolds number; this that simplifies its interpretation.

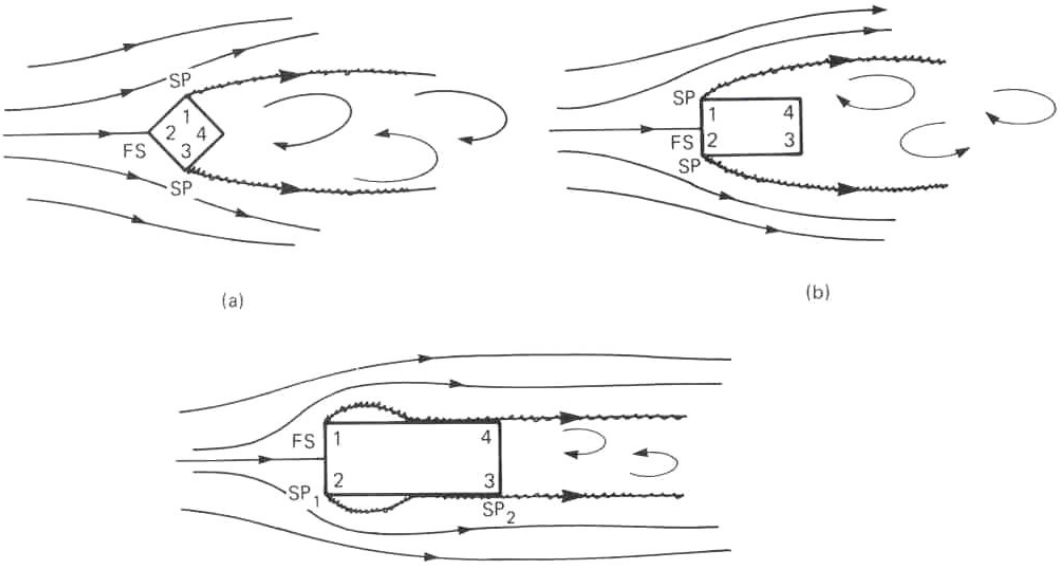

Figure 34

Figure 35 shows the qualitative trend of the drag coefficient of the body on varying the ratio between the width b and the depth h of the section. At first, with the increase of b/h, C_D increases reaching a maximum value equal to about 3, for b/h comprised between 0.5 and 1; in this situation the wake has maximum transverse width. Still growing b/h, the wake narrows and reduces C_D according to an uncertain and variable trend (enclosed in gray lens). The value of C_D stabilizes around the unit for b/h ≅ 4, when the wake reattaches to side walls (Figure 35c) and its width remains unchanged and equal to the width of the section.

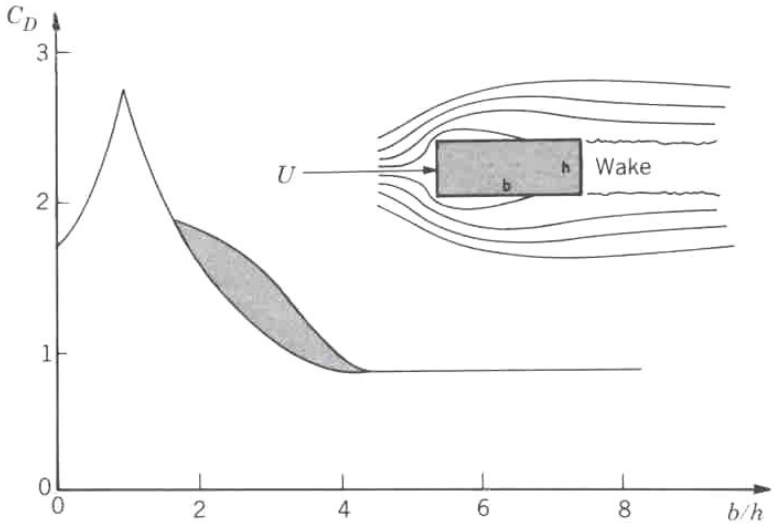

Figure 35

Figure 36 shows the variation of the drag coefficient of a square cylinder in a smooth flow as a function of Re. In fact, in the case of sharp edges (Figure 36a) C_D is almost independent of Re. Increasing the radius of curvature r of the edges, the square exhibits three distinct domains (Figure 36b), similar to those already described for the circle (Figure 31). The critical domain occurs for Re the less the greater r; the maximum retraction of the critical domain is therefore for r/h = 0.5 (Figure 36c), when the square becomes a circle. The critical domain recedes also increasing the roughness k of the surface (Figure 36c). Similar behaviors occur on increasing the atmospheric turbulence (Figure 37).

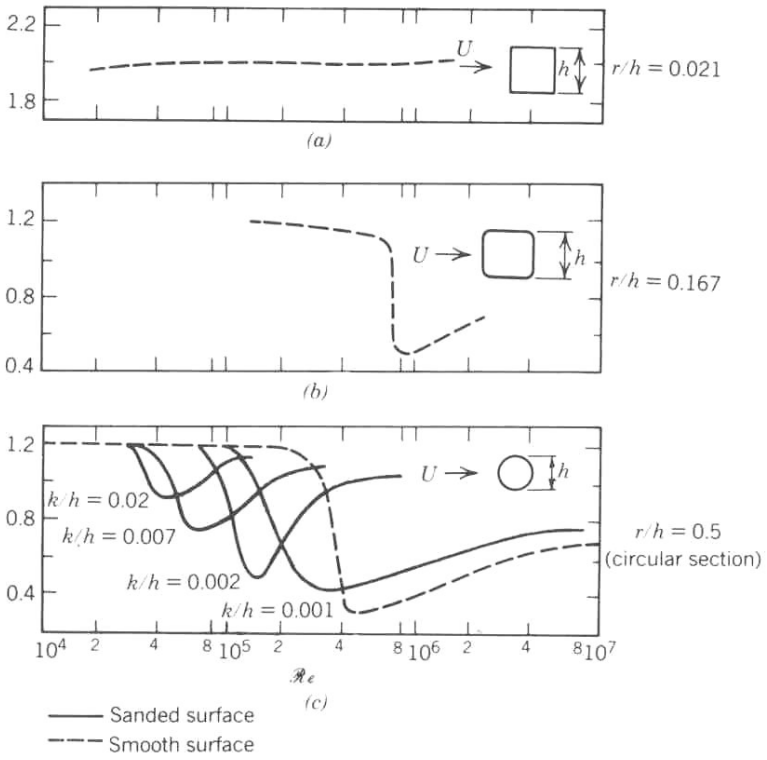

Figure 36

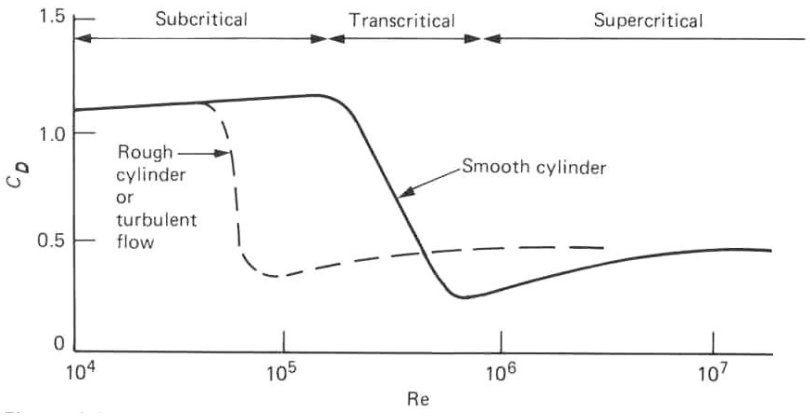

Figure 37

Figure 38 shows the coefficients C_D and C_L of various structural profiles in smooth flows.

Profile and wind direction	C_D	C_L
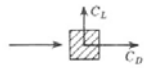	2.03	0
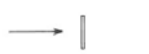	1.96 – 2.01	0
	2.04	0
	1.81	0
	2.0	0.3
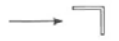	1.83	2.07
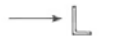	1.99	−0.09
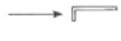	1.62	−0.48
	2.01	0
	1.99	−1.19
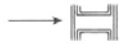	2.19	0

Figure 38

Figure 39 shows C_D and C_L for a cylinder with an octagonal section as a function of the wind direction. Figure 40 shows C_D, C_L and C_M for a bridge deck (the second Tacoma bridge) on changing the angle of wind attack. Rapid changes of C_L and C_M have an essential role in the aeroelastic behavior of structures.

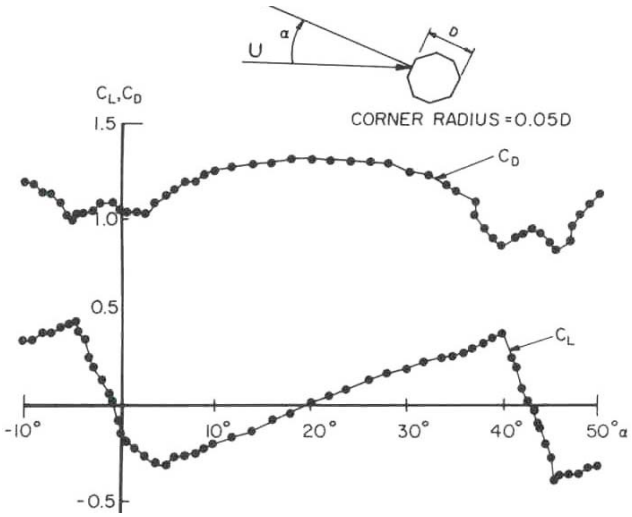

Figure 39

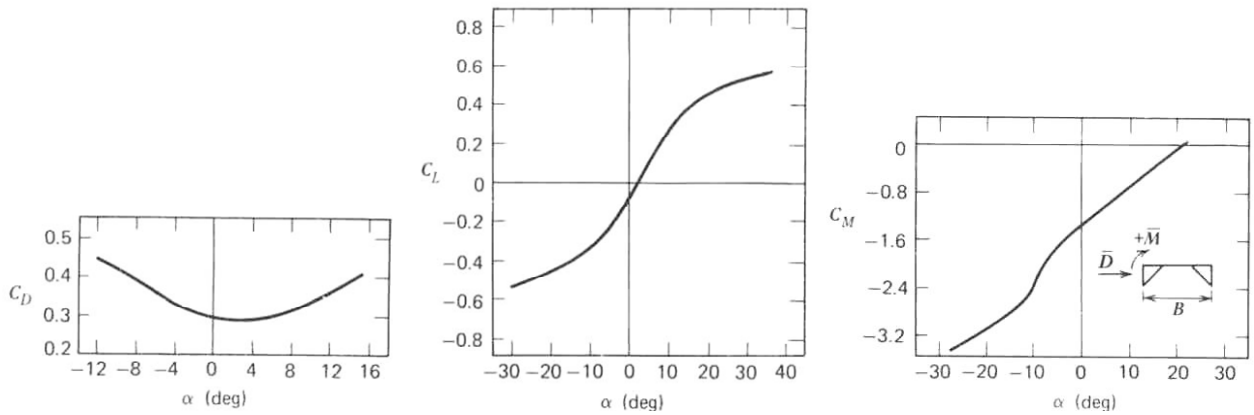

Figure 40

6. Three-dimensional bodies

The case of one-dimensional body and two-dimensional flow is ideal. However, there are many real situations where this idealization is a valuable reference. In others it is indispensable the use of models actually three-dimensional.

Let us consider initially a circular cylinder of finite length h immersed in a laminar flow field. It is subjected to aerodynamic actions less than those which would occur on a segment of length h belonging to a cylinder of infinite length. This happens since the distortion given by this body to the flow field is less than that which would occur in the ideal case because of the possibility that the fluid has to flow not only in the plane of the section of the cylinder but also to its ends (Figure 41).

The slenderness of the cylinder is essential. If the cylinder is short (indicatively h/d < 6), the end flows involve the entire wake that assumes a different configuration from the ideal case. If the cylinder is long (h/d > 10) the end flows constitute localized perturbations (Figure 42) although not negligible. At the ends the drag coefficient is reduced and a vortex arises whose shedding frequency is different from that of the wake. In the central part of the cylinder its behavior is similar to the ideal case.

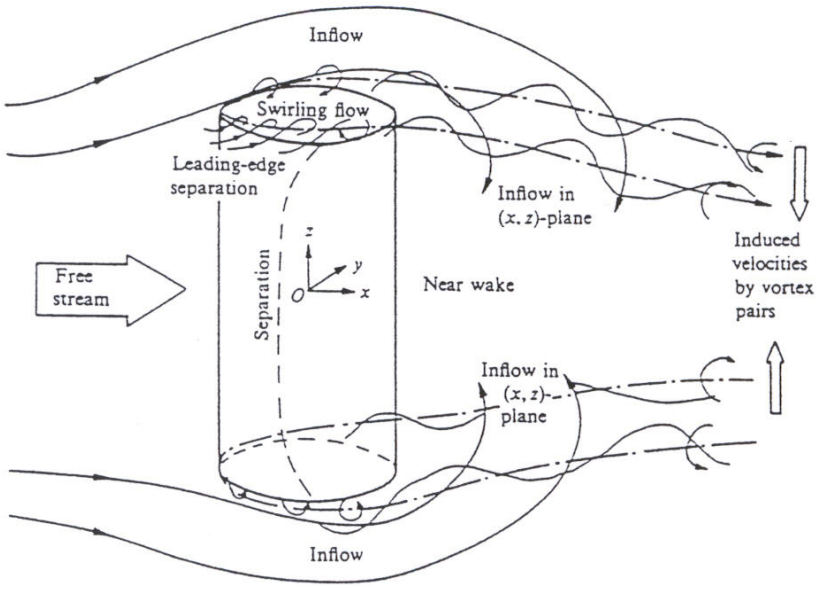

Figure 41

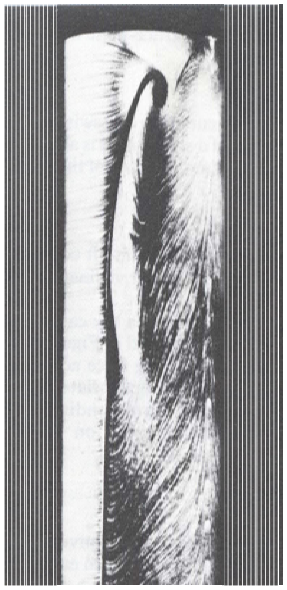

Figure 42

A second effect of three-dimensionality that does not upset the ideal behavior is that of the variability of fluctuating actions (Figure 43) along the centerline.

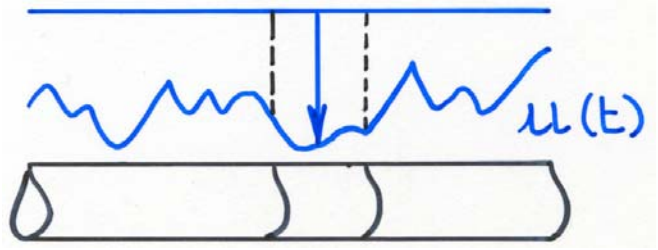

Figure 43

A third circumstance that changes the nature of the ideal flow without distorting it is the change in the mean speed of the flow (Figure 44). Engineering often deals with this problem by modelling the cylinder through a succession of strips treated, each, as blocks of an ideal cylinder. A similar situation occurs for a constant mean flow on cylindrical bodies whose section varies slowly along the centerline (Figure 45).

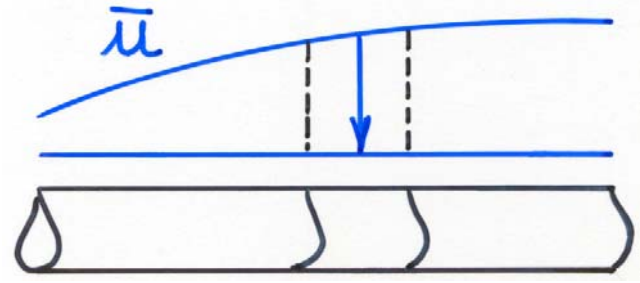

Figure 44

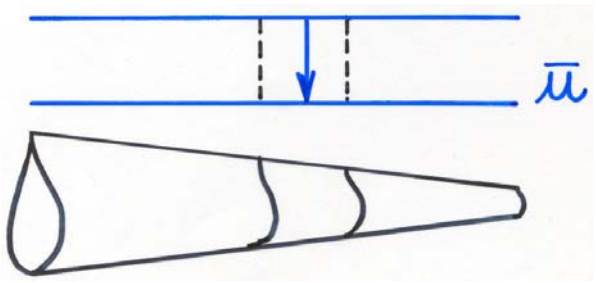

Figure 45

The simultaneous occurrence of bluff bodies, variable profile of the mean speed and the presence of turbulence results in real behaviors of complex three-dimensional nature (Figure 46). The construction reality is populated by such situations different from case to case. It is therefore necessary to carry out single experiments for each case of interest, or to formulate general criteria applicable to typological classes of buildings. This paragraph is confined to the aerodynamics of buildings with the form of a right parallelepiped. The study is done by analyzing one by one each face.

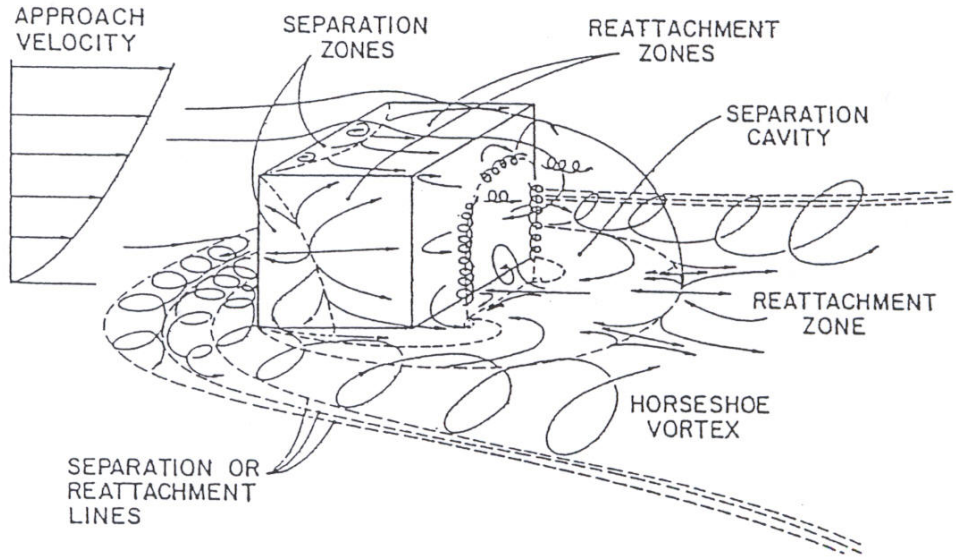

Figure 46

Starting from the analysis of the windward face, let us consider initially the presence of a constant vertical profile of the mean wind speed (Figure 47a) and the presence of fictitious constraints that force the flow to maintain its horizontal direction. For the Bernoulli law the pressure coefficient on this face is unitary and the pressure is constant (Figure 47b). From a physical point of view this is the situation that occurs when the flow, rather than investing a full plate (Figure 48a), through a grate (lattice plate) with high open area ratio (Figure 48b).

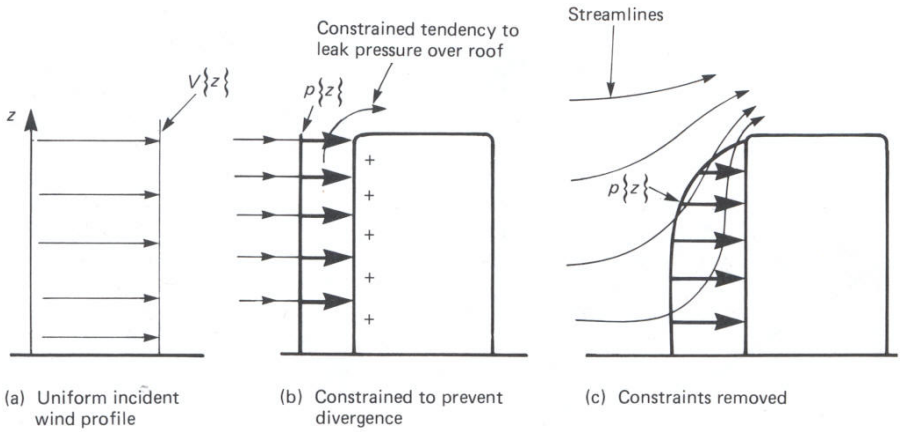

Figure 47

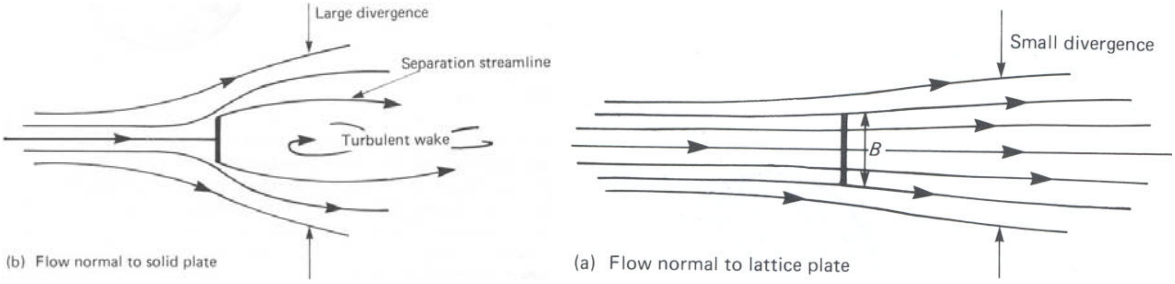

Figure 48

Removing the fictitious constraint the flow envelops the lateral edges and the upper face (Figure 46). Figure 47(c) shows that the streamlines deviate upward while the pressure is reduced at the upper edge. This behavior occurs in wind tunnel tests that provide a uniform smooth flow (aeronautic wind tunnels).

Let us consider the case in which the mean speed varies with height according to the principles of the atmospheric boundary layer (Figure 49a) and fictitious constraints are imposed again. The pressure coefficient is unitary and the pressure increases with height (Figure 49b). Removing the constraints there is a stagnation point along the median line of the face, at about 2/3 the building height. The streamlines deviate laterally along the lateral edges; above the stagnation point they deflect upward causing a local reduction of the pressure coefficient (Figure 49c); below the stagnation point the pressure gradient induces a downward flow that produces a vortex at the base of the building; it changes the pressure at the base (Figure 49c).

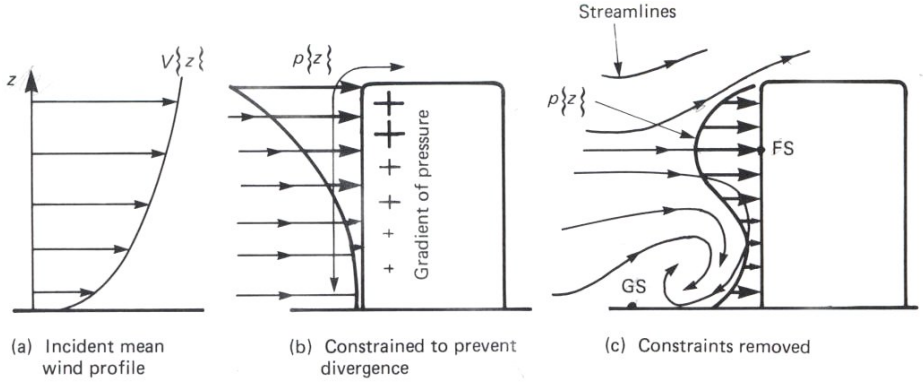

Figure 49

Figure 50 illustrates the distribution of the pressure coefficient on the windward face in the case of uniform flow (Figure 47c) and with variable profile (Figure 47c, the reference speed is constant and equal to its value at the building top). The difference confirms that the transition from one-dimensional to three-dimensional bodies tends to reduce aerodynamic actions. It also confirms that wind tunnels producing uniform flows are not suitable for the aerodynamic testing of buildings.

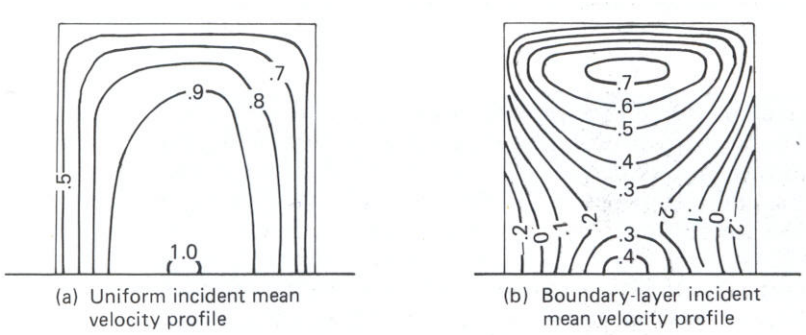

Figure 50

Figure 51 shows the separation of the flow along the lateral edges of the windward face. In the upper part A the flow speed remains comparable to that of the oncoming flow. In the lower part B the flow accelerates and takes on the typical shape of a train of "horseshoe" vortices (Figure 46). The sides are in depression as the leeward face. Behind this face the wake is organized into two structures called "near-wake" and "far-wake" (Figure 52). The first is a recirculation flow in contact with the leeward face; the latter gives rise to a train of vortices that migrate downstream up to mix with the turbulence of the atmospheric flow field.

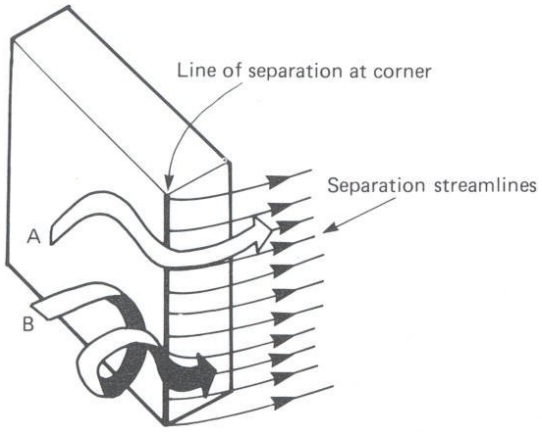

Figure 51

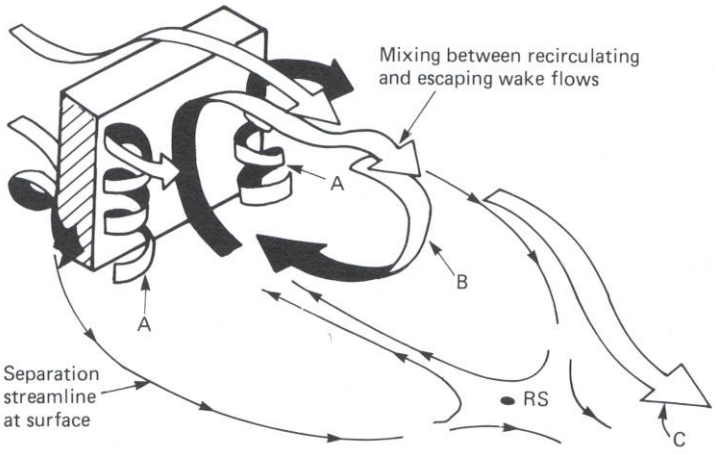

Figure 52

The separation phenomena involving the roof are often essential in the behavior of low-rise buildings.

Let us consider first the case in which the flow is orthogonal to the windward face and the roof is flat and horizontal. In the case of homogenous flow (Figure 53a) the separation takes place along the upper edge of the windward face and, unless roofs very elongated, is kept separate, leaving the entire roof in a homogeneous state of

depression (Figure 54a). In the case of buildings in the atmospheric boundary layer (Figure 53b) the Reynolds stresses linked with the atmospheric turbulence favor an early reattachment of the wake at the rear of the roof (Figure 54b); the pressure distribution on the roof in the wind direction is approximately linear, with a maximum negative value at the edge of the separation and very small values (sometimes positive) in the back.

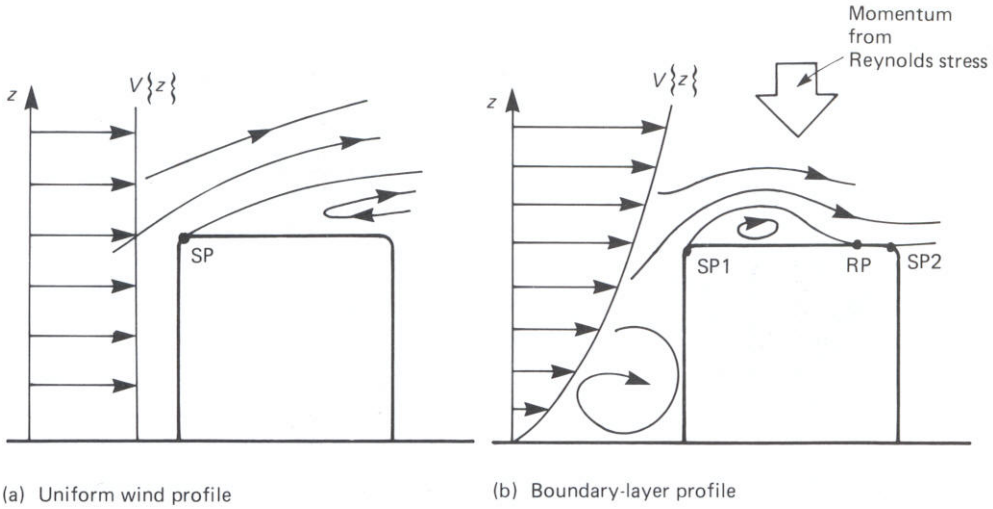

Figure 53

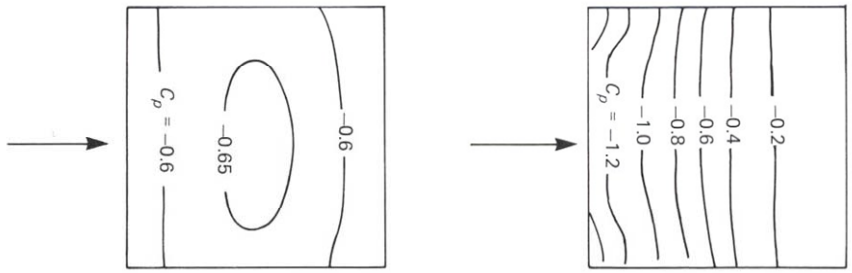

Figure 54

Maintaining the flow direction orthogonal to the windward face, the change of the slope on the horizontal of the roof causes different flow regimes (Figure 55). Another kind of change occurs in the behavior of flat roofs when the direction of the oncoming flow changes. Figure 56(a) shows the typical occurrence of a vortex pair along the front edges of the roof, when the flow is directed diagonally. Figure 56(b) shows the high state of depression concentrated at the corner of the roof. Architectural finishing edges (eaves, parapets, shaping ..) modify and generally reduce these phenomena.

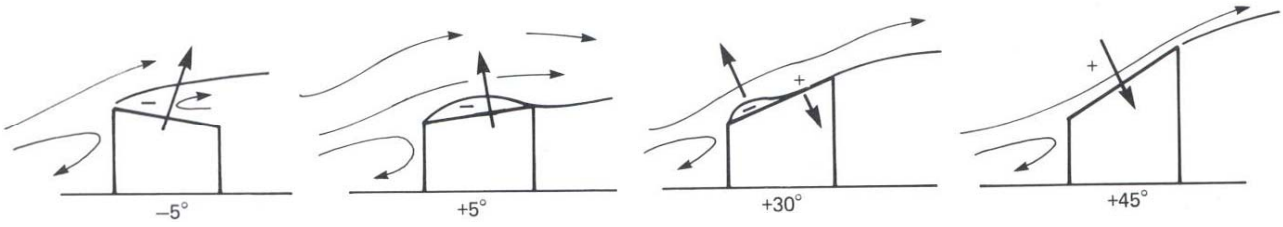

Figure 55

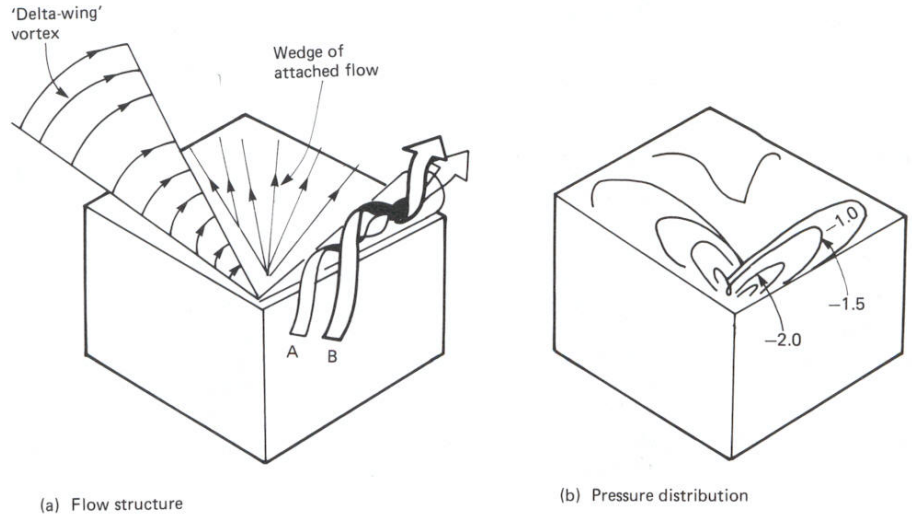

Figure 56

7. Overall and local aerodynamic actions

The wind causes overall aerodynamic actions on buildings and local aerodynamic actions on individual elements, structural or not, that make up the construction.

The overall aerodynamic actions are normally assessed assuming as oncoming wind directions those of the main axes in plant (Figure 57). For square towers it should be also considered the possibility that wind blows in the diagonal direction (Figure 58). For structures with a symmetry axis or lacking of symmetry axes all oncoming wind directions should be considered.

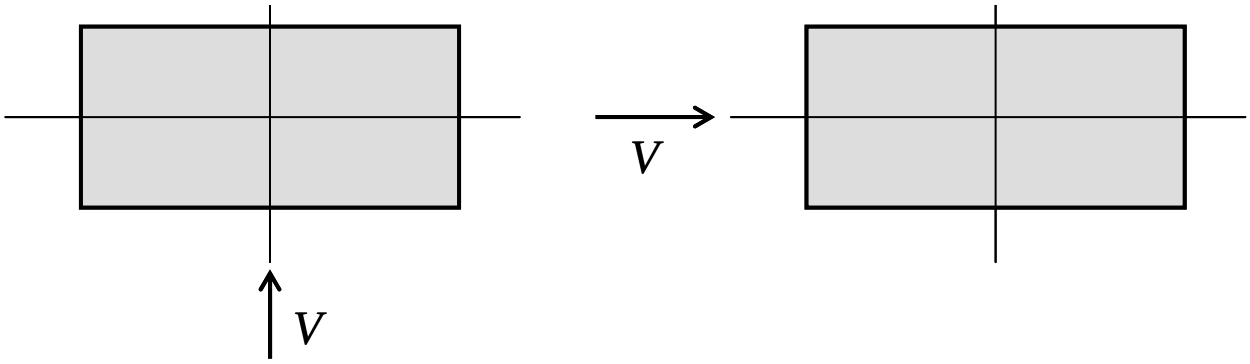

Figure 57

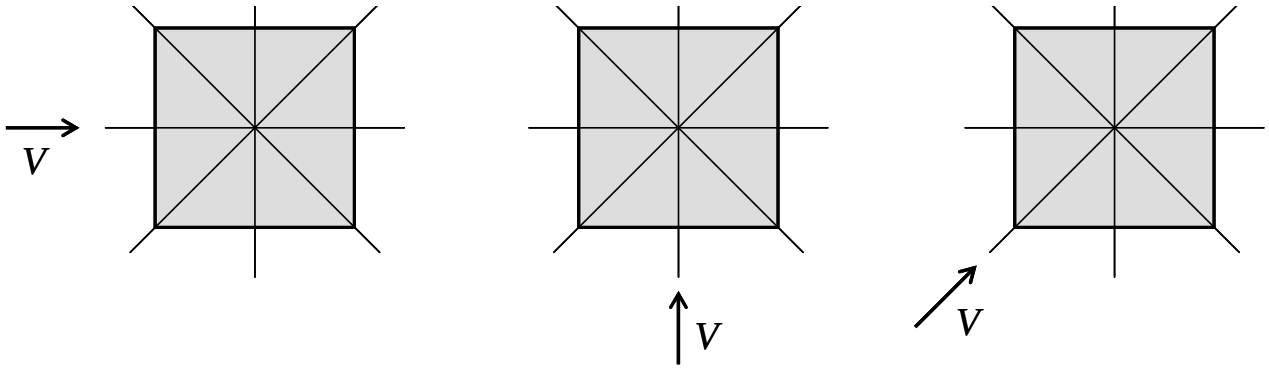

Figure 58

The aerodynamic coefficients that transform the velocity pressure of the undisturbed wind into overall aerodynamic actions are called overall aerodynamic coefficients.

Local aerodynamic actions premises on individual elements are assessed for all the possible wind directions. Especially at the edges and corners (Figure 59) they are often much higher than those applied on the individual elements to evaluate overall actions. Moreover, taking into account the partial correlation of wind pressures, they are all the more intense the smaller the area of the surface on which they are applied.

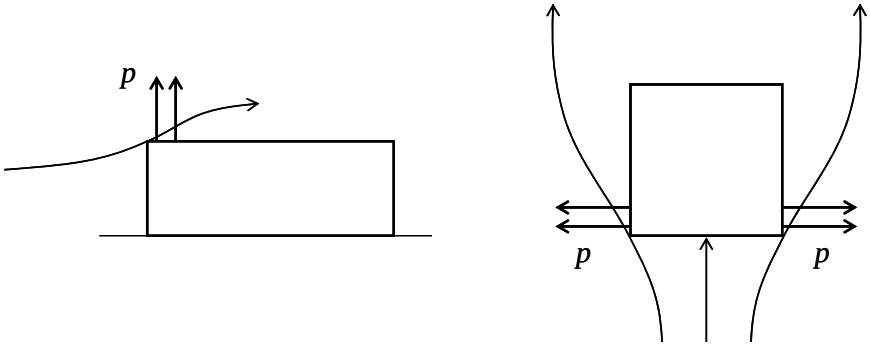

Figure 59

The aerodynamic coefficients that transform the velocity pressure of the undisturbed wind into local aerodynamic actions are called local aerodynamic coefficients. They are generally employed to evaluate wind actions on individual covering elements and their fasteners (cladding, facade elements, components, cover, etc).

The pressures of overall and local pressures are never combined.

Figure 60 shows a typical damage suffered by windows in the corner of a building, caused by the intense suction due to wake separation.

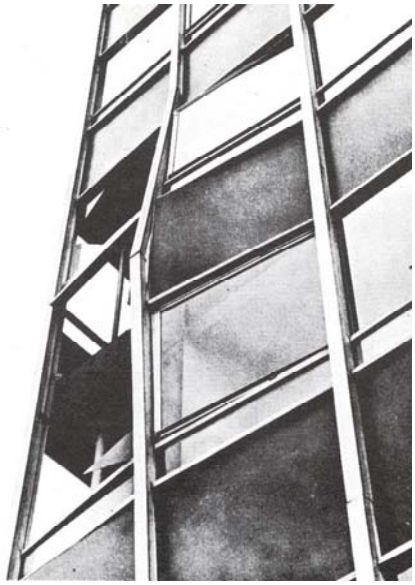

Figure 60

Figures 61 and 62 show a typical damage to the linings of the roofs of single-story buildings, caused by the intense suction due to the wake separation.

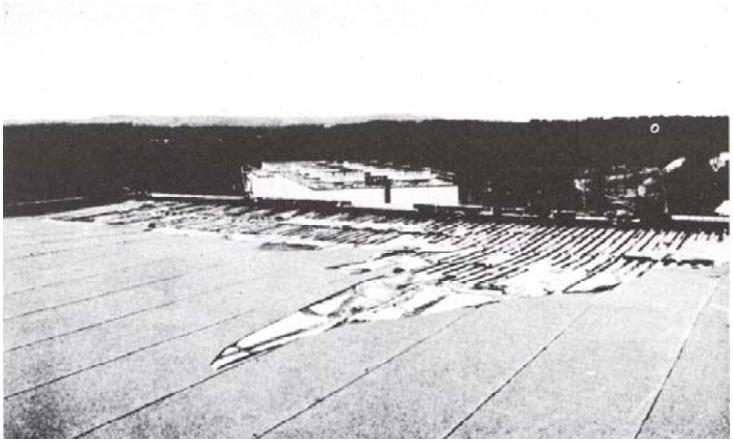

Figure 61

Figure 62

Figure 63 shows the damage suffered by the coating coverage of a building due to the intense suction due to the wake separation and the formation of a pair of conical vortices.

Figure 63

The increase in local pressure in areas where the separation of the vortex wake takes place is greatly enhanced by the non-Gaussian character of these pressures.

Figure 64 shows the distribution of the mean pressure coefficients on the four sides of a tall building. In a similar way Figure 65 shows the skewness and the kurtosis of the pressure coefficients. On the windward side they tend respectively to the values 0 and 3 of the Gaussian distribution. On the other faces they are very different from these values, confirming the non-Gaussian character of pressure.

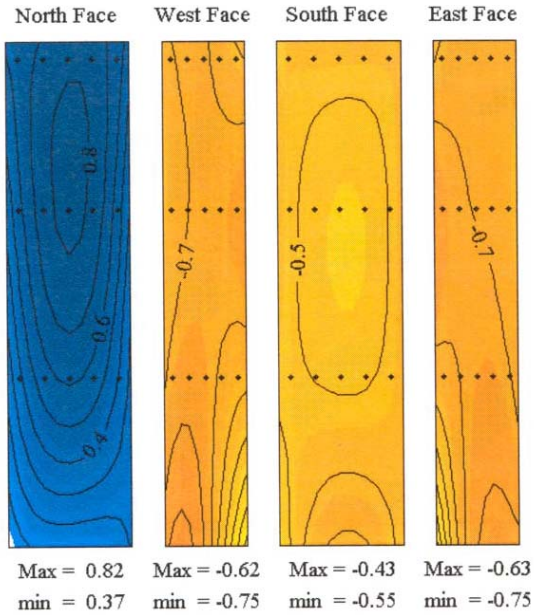

Figure 64

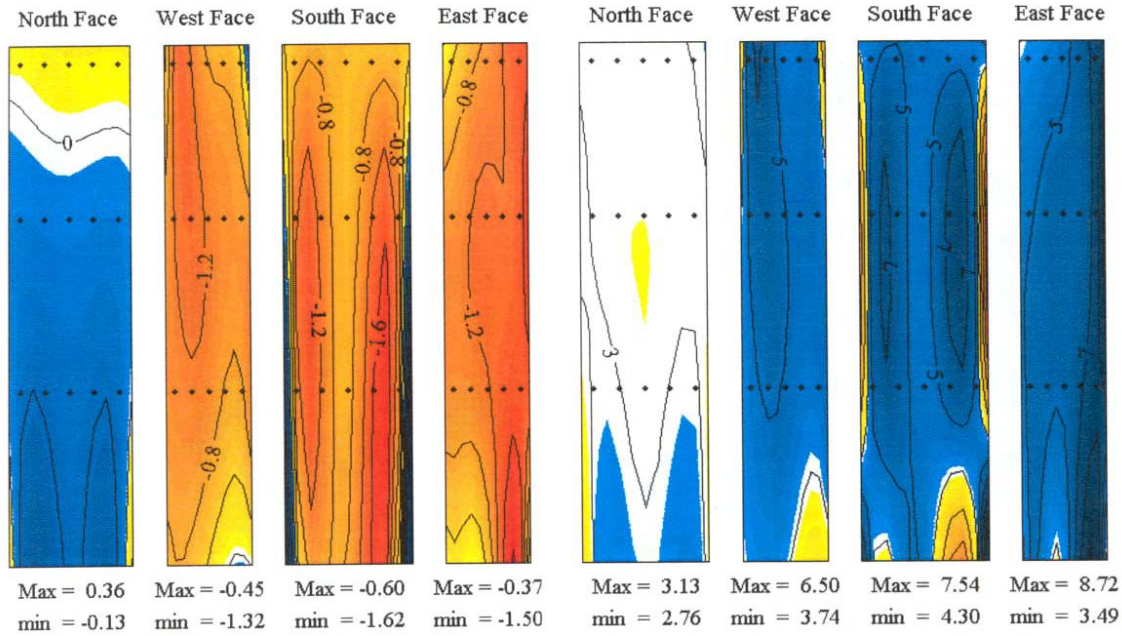

Figure 65

Figures 66(a) and (b) show the instantaneous pressure coefficients, as a function of time, in a central area of the windward face and in an area of the side face at the edge from which separation occurs. Figures 67(a) and (b) show the relative histograms,

comparing them with the Gaussian density function. On the windward side the pressure is Gaussian; in proximity of the lateral edge it clearly deviates from this condition. Figures 68(a) and (b) show that the deviation from the Gaussian distribution has a great impact on the distribution of the maximum value (in absolute value); this interprets and justifies the enormous growth of the peaks.

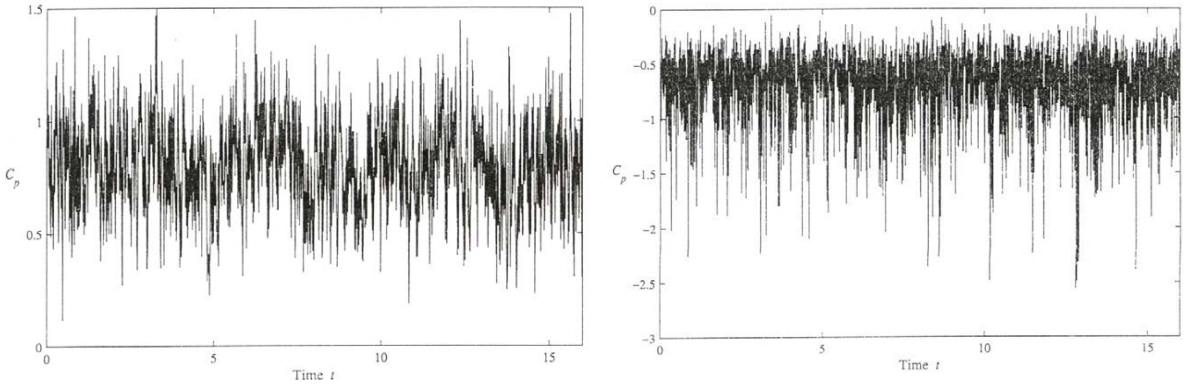

Figure 66

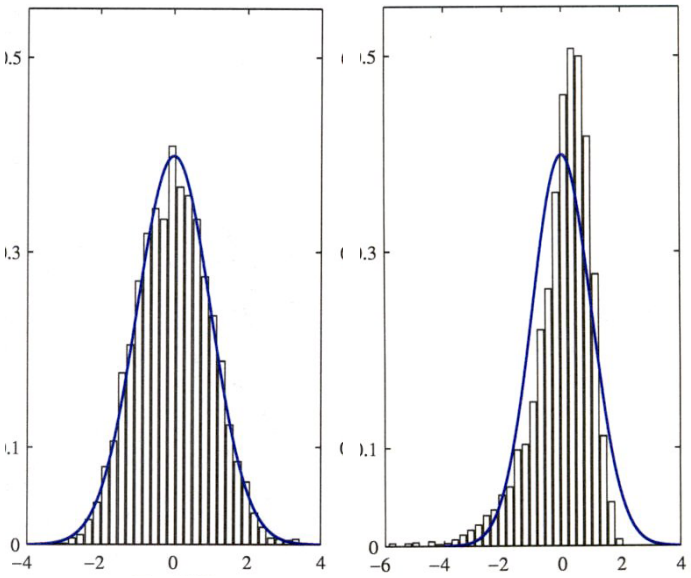

Figure 67

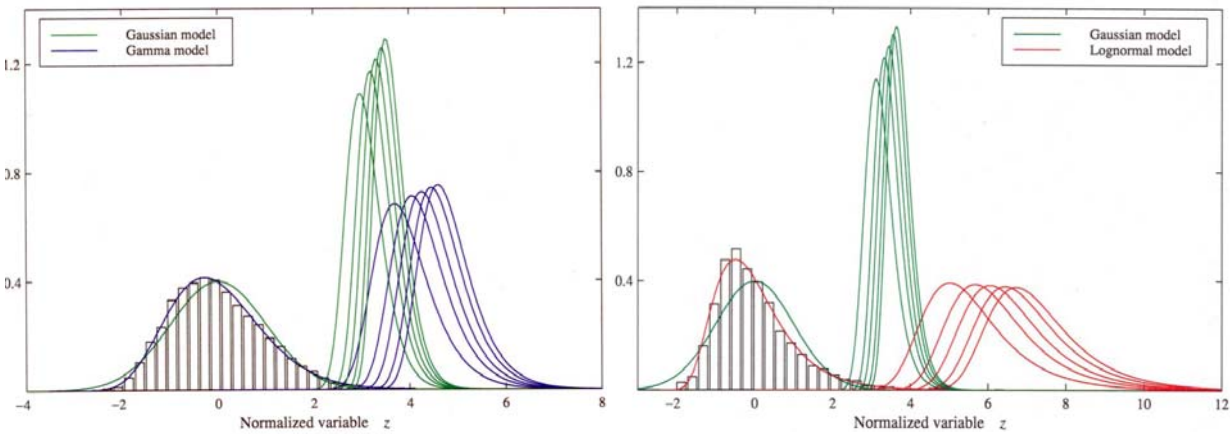

Figure 68

8. Internal pressure

While external pressures vary on the outer surface of buildings, internal pressures are uniform in all the inner linked spaces. Their value is determined by the number, the position and size of the openings (doors, windows, distributed cracks, ...), that is the connections between the external and the internal environment.

Figure 69 shows four typical situations.

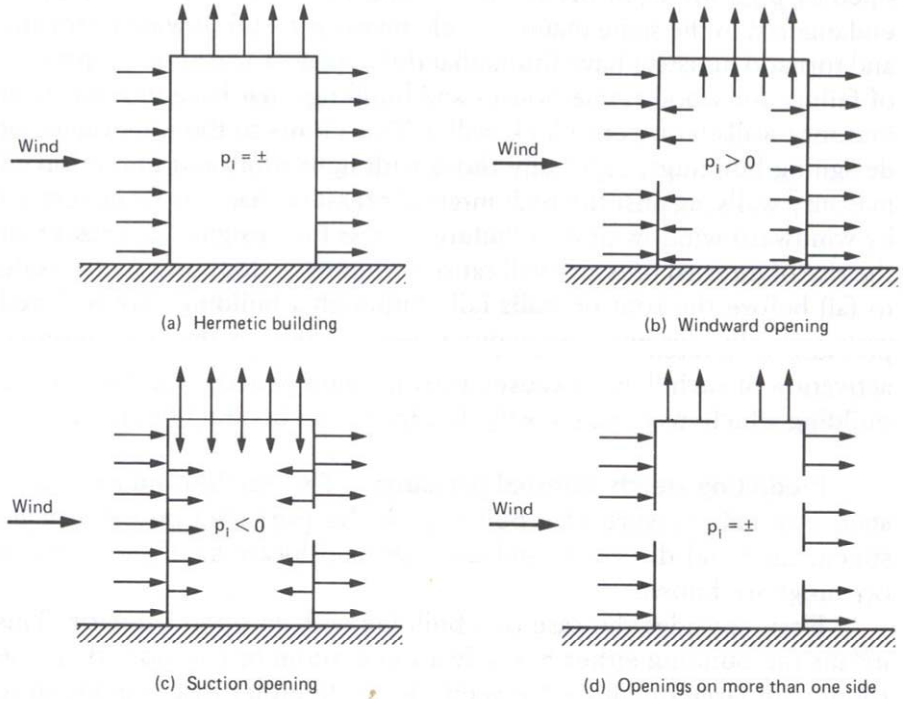

Figure 69

In Figure 69(a) the building is hermetically closed and the internal pressure does not depend on the external one. It has a value p_i that depends on the initial conditions. Except in special cases, in the engineering practice $p_i = p_o$.

In Figure 69(b) there is a single opening in the windward face, where the external pressure is positive. The internal pressure assumes the same positive value and gives rise to burdensome actions on the side walls, on the leeward wall and on the roof. The worst case is realized when the opening is placed in the stagnation point.

In Figure 69(c) there is a single opening in the leeward wall where external pressure is negative. The internal pressure assumes the same negative value and gives rise to burdensome actions on the windward wall. The worst case occurs when the opening is placed at the edges of the cover (an open skylight, a broken glass, ...).

In Figure 69(d) the openings are distributed on all the sides of the building. In this case the internal pressure depends on the number, size and distribution of openings. If the openings with greater surface are located on the windward wall the internal pressure is positive. If, instead, the open surfaces prevail on the walls in suction, the internal pressure is negative. In any case, the internal volume is characterized by intense circulation phenomena between the zones of different pressure.

Figure 70 illustrates typical damage due to positive internal pressure on the leeward side of buildings with openings on the windward side.

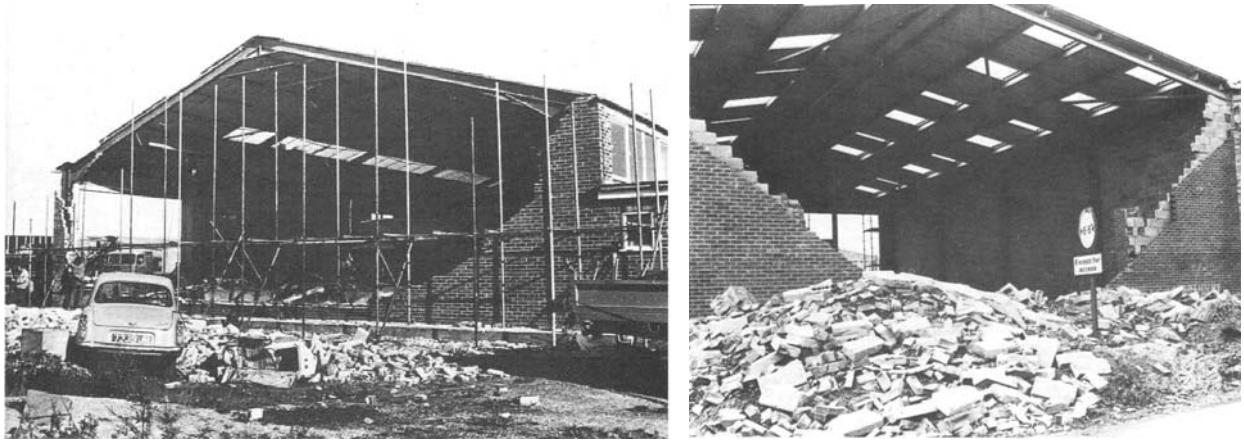

Figure 70

Let us consider a construction in a uniform flow; it is equipped with N openings and a single inner volume. Treating each opening as an orifice, the emission volume of air entering or outgoing from the j-th opening is given by the law:

$$Q_j = C_j A_j V_j = \pm C_j A_j \sqrt{2\left|P_j - P_i\right| / \rho} \tag{8.1}$$

where C_j is the emission coefficient of the orifice ($C_j \cong 0.73$ for square orifices), A_j is the area of the opening, V_j is the mean wind velocity of the air that crosses the orifice, p_j is the external pressure at the orifice, p_i is the internal pressure. The sign + denotes entering air; the sign – refers to outgoing air. The continuity equation:

$$\sum_{1}^{N}{}_j Q_j = 0 \tag{8.2}$$

expresses the balance between the volume of air in and out. The replacement of the third member of Eq. (8.1) into Eq. (8.2) gives the value of the only unknown p_i.

Let us consider the case of a building where there are two openings, one (1) on a wall in pressure, the other (2) on any one wall in depression. It results:

$$Q_1 + Q_2 = 0 \Rightarrow \quad C_1 A_1 V_1 + C_2 A_2 V_2 = 0 \Rightarrow \quad C_1 A_1 \sqrt{\frac{2\left|p_1 - p_i\right|}{\rho}} - C_2 A_2 \sqrt{\frac{2\left|p_2 - p_i\right|}{\rho}} = 0$$

Assuming that the two openings have the same shape ($C_1 = C_2$) it follows:

$$A_1^2 (p_1 - p_i) - A_2^2 (p_i - p_2) = 0 \Rightarrow$$

$$A_1^2 (p_1 - p_o) - A_1^2 (p_i - p_o) = A_2^2 (p_i - p_o) - A_2^2 (p_2 - p_o) \Rightarrow$$

$$A_1^2 C_{p1} - A_1^2 C_{pi} = A_2^2 C_{pi} - A_2^2 C_{p2} \Rightarrow \quad A_1^2 C_{p1} + A_2^2 C_{p2} = \left(A_1^2 + A_2^2\right) C_{pi} \Rightarrow$$

$$C_{pi} = \frac{A_1^2 C_{p1} + A_2^2 C_{p2}}{A_1^2 + A_2^2} \tag{8.3}$$

Finally, assuming $a = A_1/A_2$ it follows:

$$C_{pi} = \frac{C_{p2} + a^2 C_{p1}}{1 + a^2} \tag{8.4}$$

Eqs. (8.3) and (8.4) can be generalized by indicating respectively with A_1 and A_2 the overall area of the openings on the faces under pressure and in suction; p_1 and p_2 are the average values of the positive and negative pressures.

As an example, let us consider a square building in which the openings are uniformly distributed on the four side walls. Since one is in pressure and the other three are in suction, a = 1/3. In addition, $C_{p1} = 0.8$ and $C_{p2} = -0.5$. Applying Eq. (8.4) $C_{pi} = -0.37$; this shows that a uniform distribution of the openings causes a negative internal pressure.

Excluding the presence of a dominant opening and assuming that the distribution and the size of the openings is not known, standards generally provide a pair of positive and negative values of the coefficients of internal pressure.

Previous assessments correspond to steady conditions. The sudden opening of a door or of a window causes a wave of internal pressure characterized by a transient regime typical of a step force. The values of the internal pressure that take place in this phase may come to be double those in the previous scheme. This can produce aerodynamic actions of short duration but high intensity. Figure 71 shows two stories of pressure associated with sudden openings or closings.

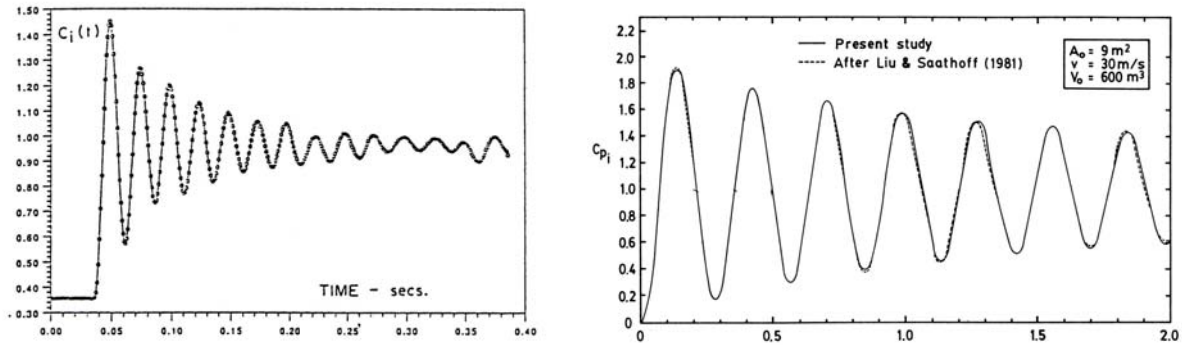

Figure 71

9. Interference

The concepts developed so far are based on the tacit assumption of isolated bodies. In fact bodies are never isolated. They are surrounded by other bodies or are influenced by discontinuity surfaces, such as the floor on which they rest. At most it can be said that a body can be treated as isolated if the boundary elements have a marginal influence. It is defined as interference the whole phenomena that deviate from this ideal situation. It involves changes of the flow field and the aerodynamic actions that, depending on cases, may be reduced or enhanced.

Figure 72 illustrates this concept showing how a small circular bar, before a square cylinder, changes the flow and the wake of the cylinder.

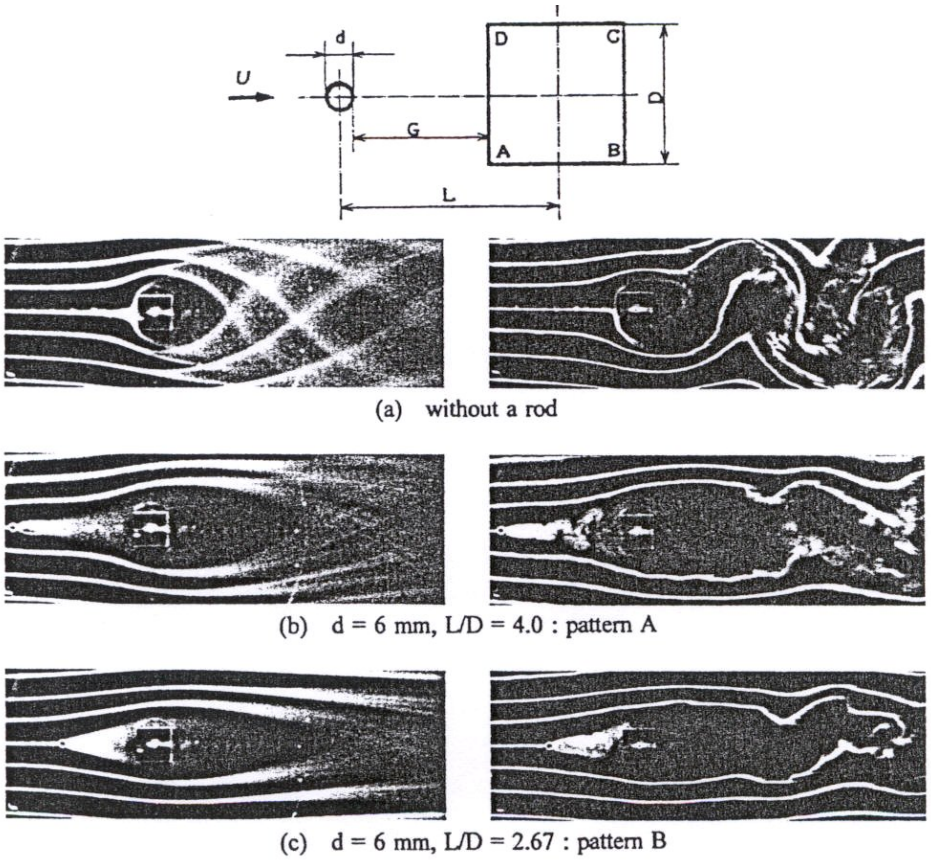

Figure 72

To provide a complete picture of the interference phenomena is almost impossible. The situations and parameters in play in reality are too much numerous and different from case to case. Once again it is therefore necessary to carry out individual tests, or to formulate general criteria for typical classes of behaviors.

Figure 73 shows a one-dimensional circular cylinder in proximity of a boundary surface parallel to the flow (for example, an underwater pipeline). If the cylinder was isolated ($H/D \rightarrow \infty$), the symmetry of section would nullify the mean lift coefficient. It grows instead on reducing H/D (Figure 73a); in the meanwhile the drag coefficient decreases (Figure 73b) up to a minimum of 50% when the cylinder rests on the floor.

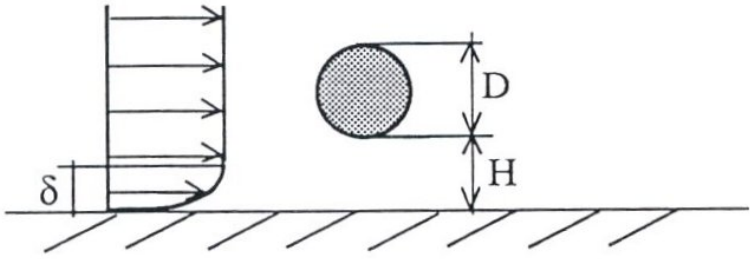

Figure 73

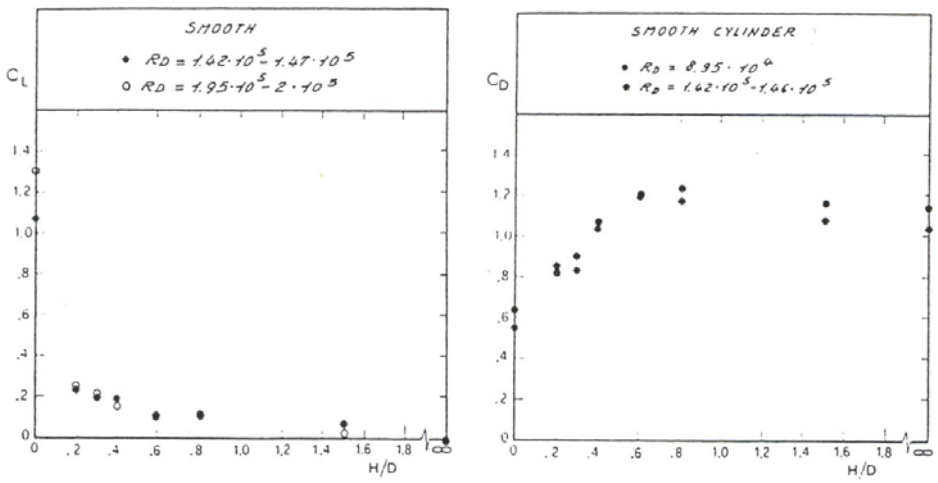

Figure 74

Figure 74(a) shows two cylinders placed side by side transversely to the current. For 1 < t/D < 1.2 a single wake is formed that detaches alternating vortices as if the cylinders were one body (Figure 74b). For 1.2 < T/D < 2-2.2 there is a bi-stable asymmetrical flow, with vortex wakes of different width for the two bodies (Figure 74c). For 2.7 < T/D < 4-5 each cylinder has a vortex wake of equal size, with vortex shedding alternately synchronized in phase and frequency (Figure 74d). Figure 75 shows the drag and lift (the latter always repulsive) on each cylinder.

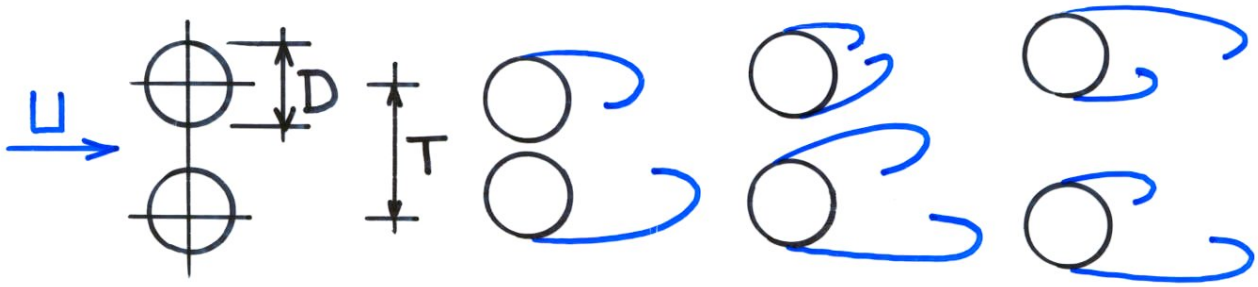

(a) (b) (c) (d)

Figure 75

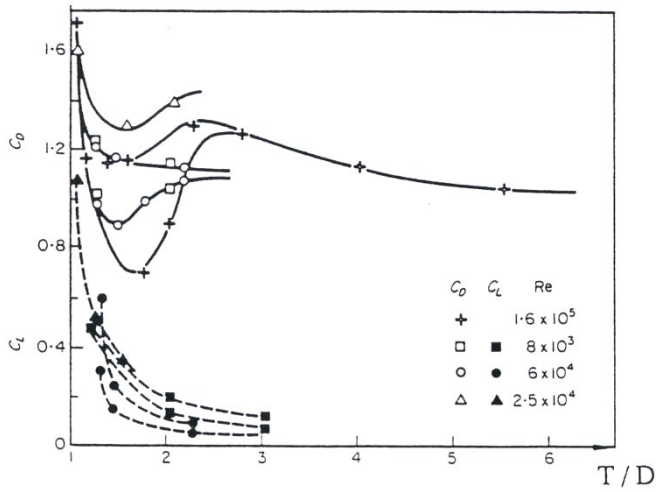

Figure 76

Figure 77(a) shows two cylinders in tandem, that is, aligned in the flow direction. For 1 < L/D < 1.2-1.8 the wake of the front cylinder includes the rear cylinder (Figure 77b). For 1.2-1.8 < L/D < 3.4-3.8 the wake of the front cylinder reattaches on the surface of the rear cylinder creating a stationary flow; behind the rear cylinder a wake of alternating vortices occurs (Figure 77c). In this situation the front cylinder is subjected to an average drag lower than that of the rear cylinder; the rear cylinder is instead subjected to an alternating vortex shedding. By contrast, the rear cylinder is subjected to a negative average drag and to an alternating force due to the vortex wake. For L/D > 3.4-3.8 both cylinders produce wakes of alternating vortices and are subjected to alternate lift forces; the rear cylinder is also subjected to high drag forces due to the vortex shedding from the front cylinder (Figure 77d).

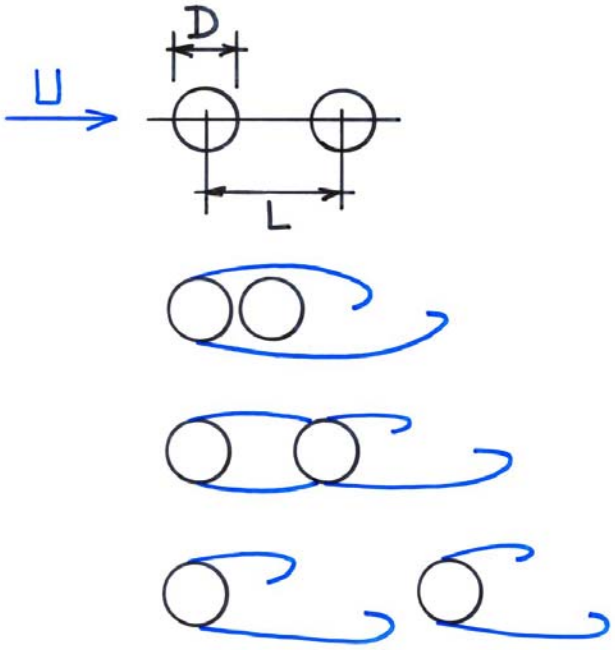

Figure 77

Figure 78 shows two staggered cylinders. Figure 79 shows the mean drag and lift coefficients on the second cylinder as a function of T/D and L/D. In a neighborhood of T/D = 0 small changes in this ratio cause great variations of the aerodynamic actions. This has an essential role in the aeroelastic behavior of the cylinders.

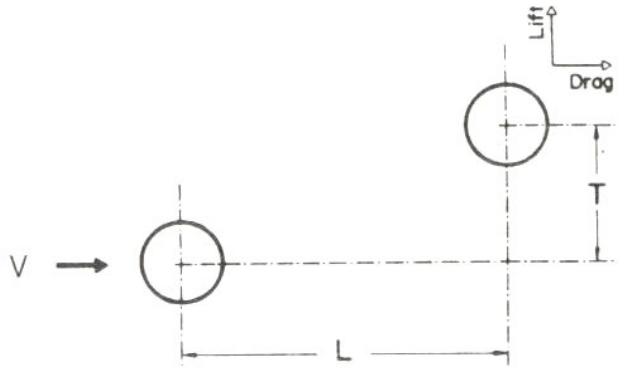

Figure 78

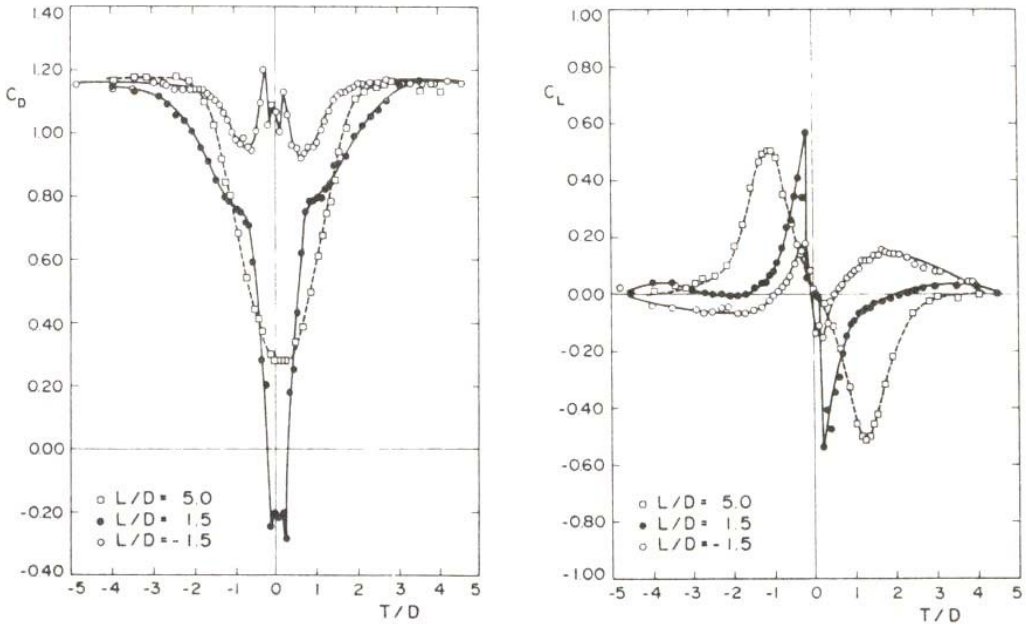

Figure 79

Figures 80 and 81 show the results of a vast campaign of experimental tests designed to assess the effects of interference between adjacent buildings with a square plan. The contour lines connect points with equal interference factor IF, where IF is the ratio between the drag coefficient of the actual building (i.e. in the presence of the other building) and the drag coefficient of the isolated one. Figure 80 illustrates the values of IF referred to the average action, proving that they are affected positively by the shielding effect of the front building. Figure 81 shows the values of IF referred to the rms actions; in this case the fluctuating component of the load manifests significant increases, especially in the presence of large building shielding.

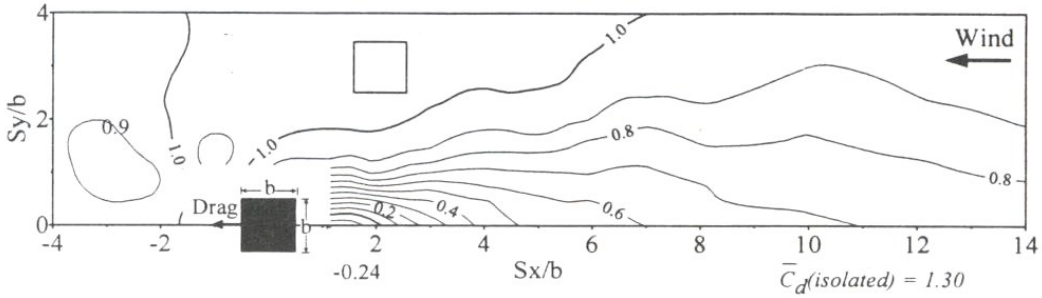

Figure 80

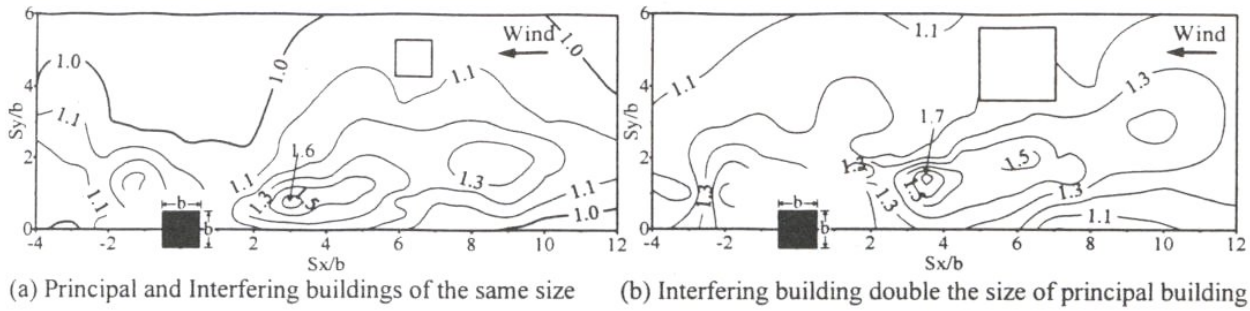

(a) Principal and Interfering buildings of the same size (b) Interfering building double the size of principal building

Figure 81